Journal of Molecular Graphics and Modelling 45 (2013) 157–172

Contents lists available at ScienceDirect

Journal of Molecular Graphics and Modelling

journal homepage: www.elsevier.com/locate/JMGM

3D-QSAR analysis of TRPV1 inhibitors reveals a pharmacophore applicable to diverse scaffolds and clinical candidates

Rajendra Kristam[a,b], Vinod Parmar[a], Vellarkad N. Viswanadhan[a,*]

[a] Department of Computational Chemistry, Jubilant Biosys Limited, #96, Industrial Suburb, 2nd Stage, Yeshwanthpur, Bangalore 560 064, India
[b] Shanmugha Arts, Science, Technology, and Research Academy, Thanjavur 613 402, Tamil Nadu, India

ARTICLE INFO

Article history:
Received 1 February 2013
Received in revised form 27 May 2013
Accepted 15 August 2013
Available online 28 August 2013

Keywords:
TRPV1 inhibitors
TRPV1 pharmacophore
Piperazinyl-aryl series
3D-QSAR analysis of TRPV1 inhibitors
Phase QSAR modeling

ABSTRACT

TRPV1 (Transient Receptor Potential Vanilloid Type 1) receptor, a member of Transient Receptor Potential Vanilloid subfamily of ion channels, occurs in the peripheral and central nervous system, and plays a key role in transmission of pain. Consequently, this has been the target for discovery of several pain relieving agents which have undergone clinical trials. Though several TRPV1 antagonists have progressed to become clinical candidates, many are known to cause temperature elevation in humans, halting their further advancement, and signifying the need for new chemotypes. Different chemical classes of TRPV1 antagonists share three important features: an amide or an isostere flanked by an aromatic (or fused aromatic) ring with polar substitutions on one side, and a hydrophobic group on the other. Recent work identified new series of compounds with these and additional features, leading to improvement of properties, and development of clinical candidates. Herein, we describe a 3D-QSAR model ($n = 62$; $R^2 = 0.9$ and $Q^2 = 0.75$) developed from the piperazinyl-aryl series of compounds and a novel 5-point pharmacophore model is shown to fit several diverse scaffolds, six clinical candidates, five pre-clinical candidates and three lead compounds. The pharmacophore model can aid in finding new chemotypes as starting points that can be developed further.

1. Introduction

Vanilloid receptor-1 or Transient Receptor Potential Vanilloid subfamily, member 1 (VR1 or TRPV1) belongs to the class of Transient Receptor Potential (TRP) family of ion channels [1]. TRPV1 is predominantly expressed in sensory neurons, and is involved in detection of painful stimuli, making it a target for developing pain-mitigating drugs [2–7]. TRPV1 is activated endogenously, by agents generated as a result of tissue injury, diabetic neuropathy, arthritis, or inflammation. These agents include endocannabinoid anandamide [8,9], lipoxygenase metabolites [10], lipid metabolites [11–13], heat (>42 °C) [14,15] and low pH (pH < 5) [16]. TRPV1 is also activated by some exogenous compounds like the vanilloid capsaicin, an active component of chili pepper, and its highly potent analog, resiniferatoxin. These exogenous agonists produce analgesic effect by hyper-stimulation of the receptor leading to long term desensitization of sensory neurons. The clinical use of such agonists is limited because of their side effects of burning sensation, irritation, edema and neurotoxicity, due to continuous influx of Ca^{2+} ions in cells [17,18]. Antagonists of TRPV1, however, produce the analgesic effect while precluding the neurotoxicity associated with activation and subsequent desensitization of the nerve cells [19–21]. In a recent review, Gavva and Wong [22,23], classified TRPV1 antagonists into four profiles, based on how they modulate TRPV1 activation by different modes such as capsaicin, pH 5 and heat.

One of the extensively studied classes of TRPV1 antagonists is BCTC (*N*-(4-tertiarybutylphenyl)-4-(3-cholorphyridin-2-yl)tetrahydropyrazine-1(2*H*)-carbox-amide) [24–26], that is based on piperazine-1-carboxamide. Various SAR as well as QSAR studies were carried out on different series of compounds (References of published SARs are in Supplementary Material, Table S2). The first 3D-QSAR models of TRPV1 antagonists dealt with cinnamide series [27] based on CoMFA [28] and CoMSIA [29], showed good predictive power and related the models to docked conformations of compounds in a TRPV1 homology model (TM3/TM4 helices). However, this series cannot be considered druglike and reversible, due to the presence of covalent bond-forming Michael acceptors. A descriptor-based QSAR model of a set of heteroaromatic urea compounds [30], developed using genetic function approximation (GFA) and partial least-squares (PLS) algorithms, correlated three descriptors, namely, number of rings, molecular volume and *kappa* shape indices to the *in vitro* activity of antagonists. A

* Corresponding author at: Jubilant Biosys Ltd., #96, Industrial Suburb, Second Stage, Yeshwanthpur, Bangalore, Karnataka 560022. Tel.: +91 80 6662 8908; fax: +91 80 6662 8333.
E-mail address: vellarkad_viswanadhan@jubilantbiosys.com (V.N. Viswanadhan).

1093-3263/$ – see front matter © 2013 Elsevier Inc. All rights reserved.
http://dx.doi.org/10.1016/j.jmgm.2013.08.014

descriptor-based QSAR [31], based on a set of aligned carboxamides, indicated that the cLogP and the hydrophilic component of the solvent accessible surface area correlate with the corresponding functional activity of the antagonists. 3D-QSAR modeling of a set of dihydroxytetrahydrobenzazepines, tetrahydroisoquinolines and arylalkyl thiourea compounds [32] based on CoMFA and CoMSIA, were used to derive steric and electrostatic fields around the scaffolds. A set of diverse TRPV1 antagonists were used to build a qualitative PHASE [33] pharmacophore model having three features and further analyzed the compounds by docking in an earlier homology model [34].

Given the number of failed clinical studies in this area, there is a strong need to obtain a general pharmacophore to guide the design of new TRPV1 inhibitor chemotypes. To our knowledge, there has been no report of a predictive and quantitative 3D-QSAR and pharmacophore model developed for druglike, reversible TRPV1 antagonists. The present report describes a 3D-QSAR model of a promising, druglike, piperazinyl-aryl series and establishes a novel pharmacophore model, using the Phase module of Schrödinger [33] package. It is shown that the derived pharmacophore model is applicable to different scaffolds of TRPV1 antagonists, which include six clinical candidates, five pre-clinical candidates and three lead compounds.

2. Pharmacophore and 3D-QSAR modeling

BCTC is a well-studied TRPV1 antagonist, based on a piperazine-1-carboxamide template. Several companies have disclosed structures related to BCTC chemotype [35–40], including a series of constrained analogs. Herein, we consider a set of 98 TRPV1 antagonists taken from literature: 4,6-disubstituted benzimidazoles [41] and 4,5-biaryl-substituted imidazoles [42], along with activity data, for developing pharmacophore-based 3D-QSAR models (structures and data in Table S1 of supplementary content). These two chemotypes were developed as conformationally constrained analogues of BCTC to improve bioavailability and other pharmacokinetic properties. Extensive and systematic structure–activity relationships of these two series of compounds led to the identification of potent, efficacious and orally bioavailable analogues. These series of compounds comprised a good dataset for development of pharmacophore and to explore its applicability to other chemotypes. The experimental activity reported for each compound is IC_{50} in nanomolar (nM) units for the inhibition of capsaicin-mediated $^{45}Ca^{2+}$ influx in CHO cells expressing rat TRPV1 receptor, which is herein converted to pIC50 (=−log IC_{50}) and this is used throughout to refer to the activity of compounds. Compounds for which the activity was reported for the mixture of diastereoisomers were not included in the dataset. Though compounds from other TRPV1 inhibitor series were not considered for 3D-QSAR modeling, known inhibitors of TRPV1, which were progressed as leads and clinical candidates, were used for alignment with the current pharmacophore model. The objective of this exercise is to assess the applicability of the current pharmacophore model to diverse series, including clinical candidates. If indeed, the model is applicable, it stands to reason that future series and drug candidates could emerge from this model.

The sequence of steps followed along with the workflow of pharmacophore and 3D-QSAR modeling is shown in Fig. 1. The dataset was divided into an external test set of 21 compounds and a model-building set of 77 compounds, using atom pair fingerprints for similarity assessment and *k-means* clustering [43] using CIMPL [44]. During QSAR modeling, the model-building set was further divided into a training set and an internal test set in the ratio of 80:20 on a random basis, resulting in 62 compounds in the training set and 15 compounds in the internal test set. Technical details of pharmacophore and QSAR modeling using Schrodinger software are given at the end, in the experimental section.

Table 1
Results of 3D-QSAR model for the training, internal test and external test/validation sets.

Statistical parameters	Model
Training set	
# of compounds in training set	62
# of compounds in internal test set	15
# of PLS factors	3
SD	0.32
R^2	0.93
F-value	273.4
p-value	$3.56E^{-34}$
RMSE	0.60
Q^2	0.75
Pearson-*R*	0.90
External test/validation set	
# of compounds	21
$R^2_{predicted}$	0.70
SD	0.31
RMSE	0.56
Pearson-*R*	0.87

3. Results and discussions

The models reported in the present work employ Phase 3D QSAR formalism, a relatively recent development [45,46], which has some advantages relative to older approaches, in generating multiple hypotheses. For example, Phase, REMOTEDISC [47] and EGSITE2 [48] generate multiple hypotheses for binding modes based on conformational sampling, whereas CoMFA and CoMSIA employ user defined alignments [49]. Phase has the additional advantage of speed in execution, as the generation of multiple models is automatic. Unlike CoMFA, where a probe atom is used to calculate the van der waals and electrostatic interactions with each compound, Phase applies a tree-based partitioning algorithm to generate bit string representations of the ligands and a bi-directional clustering approach to distinguish multiple binding modes. Based on 27 actives in the dataset, several 4-point, 5-point and 6-point pharmacophore hypotheses were generated using Phase, that were used to align all compounds of the dataset and these alignments were then used to generate 3D-QSAR models.

3.1. Analysis of pharmacophore hypotheses

Among all pharmacophore hypotheses generated and tested, the 5-point hypothesis (Fig. 2A), generated the best QSAR model in terms of various statistical measures and regression contours. This pharmacophore hypothesis and the 3D-QSAR model are described below. The hypothesis was generated using **79** as the reference structure among all actives; activity threshold for actives and inactives was defined by a threshold of pIC_{50} = 6.5. The pharmacophore model has an H-bond donor feature, two hydrophobic features and two ring aromatic features.

Fig. 2(B) and (C) shows alignment of compounds of the imidazole and the benzimidazole series to the hypothesis, respectively. Extensive exploration of SAR at the 4th position of the benzimidazole led to several compounds [41] which do not align perfectly with the lead molecule **102** (see Table S1 in the supplementary information). However, the alignments clearly show that *all* the five pharmacophore features are common to both the series of compounds.

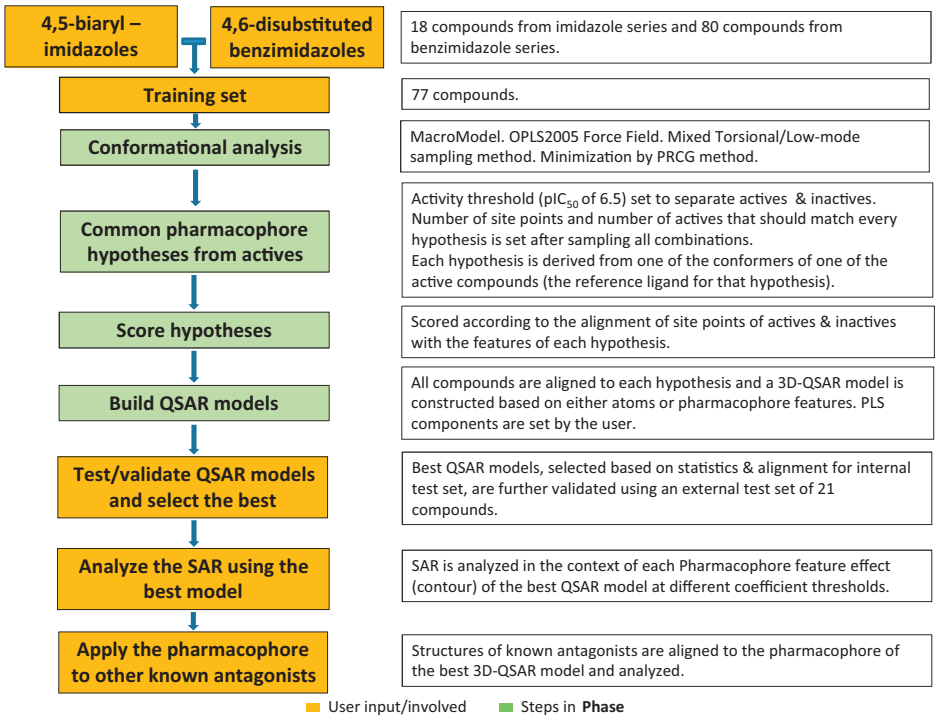

Fig. 1. Sequence of steps followed and the workflow of pharmacophore and 3D-QSAR modeling using Schrodinger/Phase.

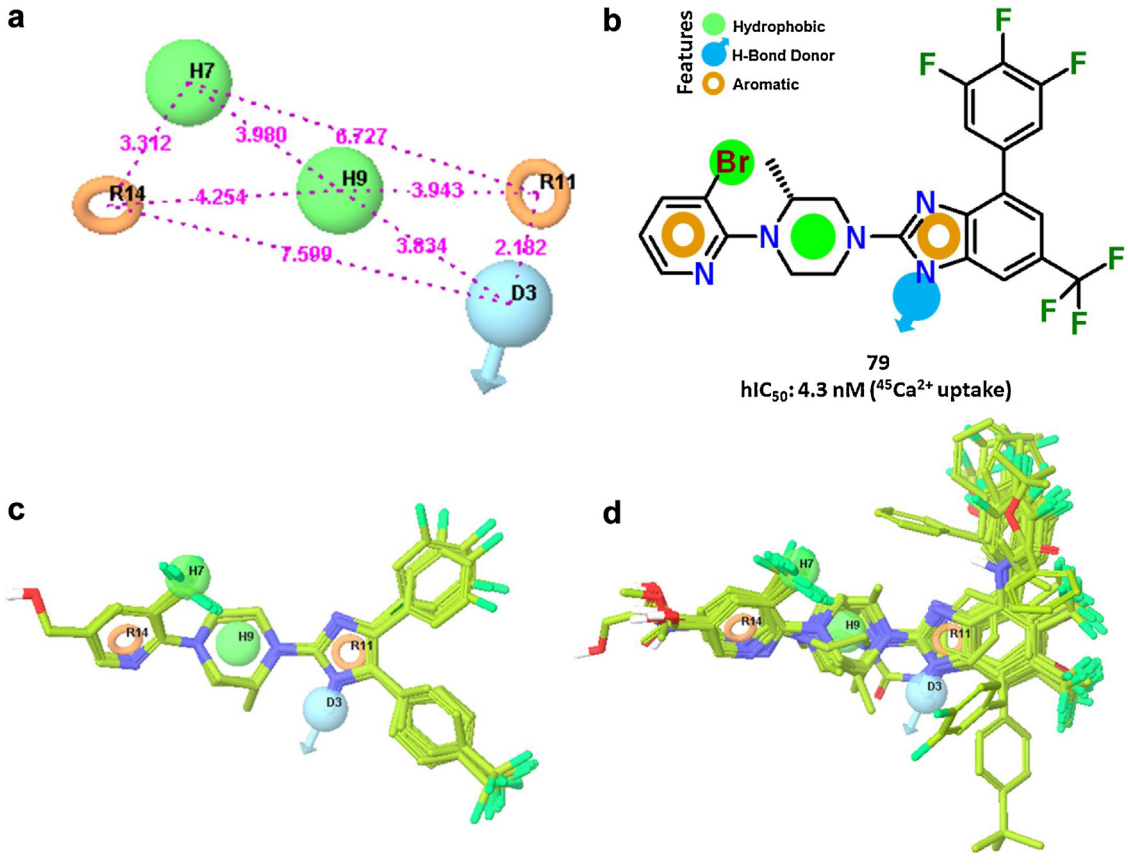

Fig. 2. (a) The 5-point pharmacophore hypothesis that gave the best 3D-QSAR model; Green represents hydrophobic feature, cyan represents hydrogen-bond donor and brown-colored ring represents a ring aromatic; All the inter-feature distances are in Angstrom (Å). (b) Chemical structure of a representative compound, **79**, along with its activity. The pharmacophore features have been schematically mapped onto the structural features they represent in **79**. (c) Alignment of active compounds of imidazole series. (d) Alignment of active compounds of benzimidazole series, using the 5-point pharmacophore hypothesis. (For interpretation of the references to color in this figure legend, the reader is referred to the web version of the article.)

Table 2
Experimental pIC_{50} values, predicted pIC_{50} values and the residuals of external test set compounds.

ID	Experimental pIC_{50}	Predicted pIC_{50}	Residual
1	6.97	6.43	0.54
6	7.36	7.62	−0.26
10	7.58	8.22	−0.63
18	5.39	5.20	0.19
21	6.88	7.48	−0.60
22	8.80	8.86	−0.06
24	8.15	8.09	0.06
28	6.24	6.20	0.03
29	7.34	7.42	−0.09
32	6.24	6.24	0.00
38	5.94	5.84	0.10
43	7.03	7.38	−0.36
44	7.01	7.41	−0.40
46	7.54	6.55	0.99
59	6.57	6.93	−0.35
64	6.74	6.12	0.62
65	5.47	6.17	−0.70
77	8.17	7.25	0.93
82	5.25	4.46	0.79
85	6.51	5.87	0.63
89	4.62	5.69	−1.07

3.2. Analysis of 3D-QSAR model

The alignment generated from hypothesis was further used to develop 3D-QSAR model, using the procedure explained in the experimental section. Table 1 shows the statistical parameters of the 3D-QSAR model generated using the hypothesis. A good 3D-QSAR model is found to be with three PLS factors and R^2 and Q^2 values of 0.93 and 0.75, respectively. Relatively high Q^2 for the internal test set compounds indicates that model is sufficiently predictive. To test the null hypothesis, Fisher ratio (F), and level of significance (p) were calculated for this model, which demonstrate statistical significance ($F = 273.4$ and $p < 0.0001$). Results indicate that, for most compounds, predicted activity values are within 1 log unit of experimental values. Other models showed poorer results overall.

3.3. Model validation by prediction of activities of external test set compounds

The 3D-QSAR model was further validated by predicting the activities of an external test set of 21 compounds that was selected from the initial dataset of 98 compounds using k-means clustering algorithm implemented in CIMPL [44]. Table 1 shows the statistical parameters for the external test set validation. $R^2_{predicted}$ for the external test set compounds is 0.70, indicating robustness of the model, and its usefulness for explaining SAR of related compounds.

The predicted pIC_{50} values of all 21 compounds of the external test set, with their experimental pIC_{50} values and residuals, are shown in Table 2. The SD and RMSE values for the external test set compounds are 0.31 and 0.56, respectively. The predicted activities of the external test set also showed a good rank correlation of 0.87. In Fig. 3 a plot of experimental and predicted activity values (pIC_{50}) is shown. The plot (Fig. 3) and Table 2 show only one outlier for the external test set, leading to a higher value of RMSE. This compound (**89**) has an ethyl ester on the terminal pyridine ring attached at the *ortho* position and is different from others in the training set in lacking a CF_3 group at *ortho* position.

3.4. Model validation by Y-randomization study

The 3D-QSAR models were developed from training and internal test sets that were formed by randomly picking compounds from the whole dataset and hence a Y-randomization or Y-scrambling study was done, generating and testing 100 models with scrambled activities, to rule out the possibility of a chance correlation [50,51]. This study established that the original model is robust and not due to any chance correlation (see Online Resource 1 for the scattered plot of Y-randomization study for the model, Figure S1).

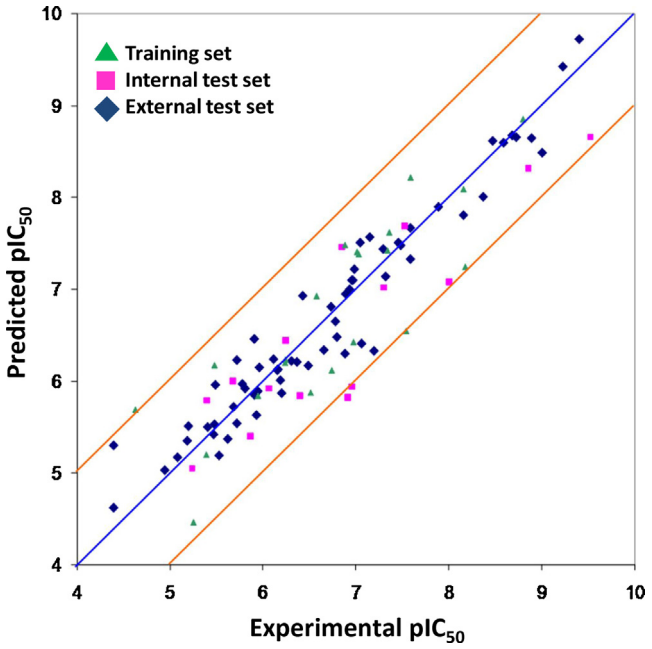

Fig. 3. Plot of experimental versus predicted pIC_{50} values of compounds for the 3D-QSAR model. Solid line represents the ideal. Dashed lines represent boundaries of 1 log unit from the ideal line.

3.5. SAR analysis by visualization of regression coefficients

Phase allows us to visualize effects due to each pharmacophoric feature and the positive and negative regression coefficients associated with the effect, like H-bond donor effects, hydrophobic effects, negative ionic effects, positive ionic effects and electron-withdrawing effects. 3D-QSAR model visualization in Phase depends on the module used. In the grid-based 3D-QSAR method used here, visualization of the model is referred to as "regression coefficient visualization" or "effects" from atom or pharmacophore types. In field-based QSAR methods, the results are represented by field "contours". In this study we looked at effects of each pharmacophoric feature – H-bond donor, hydrophobic, negative ion and positive ion – with their positive and negative regression coefficients around the pharmacophore hypothesis to visualize the favorable and unfavorable regions. In all analyses, positive coefficients and negative coefficients are shown as blue-colored and red-colored cubes, respectively.

3.5.1. Analysis of hydrogen bond donor effects

Ligand-receptor interactions inferred by the 3D-QSAR analysis can be visualized as color-coded cubes in the space around the ligand, for each of the properties considered. For the convenience and ease of viewing, the hydrogen-bond donor effects are visualized at a positive regression coefficient threshold of 0.006 and a negative regression coefficient threshold of −0.006. Fig. 4 shows active (green-colored) and inactive (magenta-colored) compounds with hydrogen bond donor effects to explain the differences in their activity. As shown in Fig. 4(A), blue-colored cubes near 5th position of pyridine ring indicate that hydrogen-bond donors in this position are favored for increasing potency of compounds. The

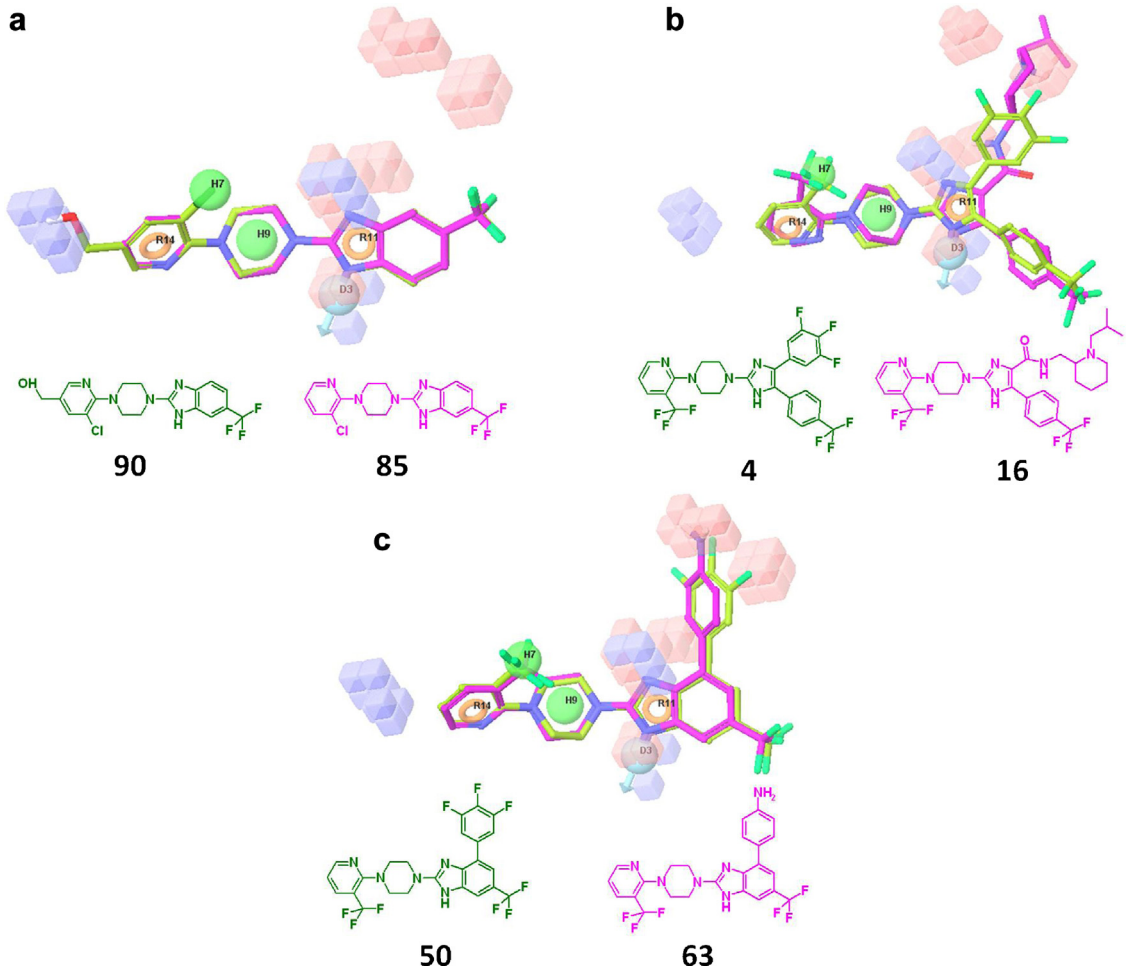

Fig. 4. Hydrogen-bond donor effects with active (green-colored stick models) and inactive compounds (magenta-colored sticks models). (a) 90 (7.19) and 85 (6.51), (b) 4 (8.15) and 16 (5.72), and (c) 50 (7.48) and 63 (5.72). The pIC_{50} values of the compounds are given in the parentheses. The cubes are as seen at a positive regression threshold of 0.006 and a negative regression threshold of −0.006. (For interpretation of the references to color in this figure legend, the reader is referred to the web version of the article.)

hydroxyl group on the 5th position of pyridine ring in the active compound (**90**; green-colored; pIC_{50} 7.19), acts as a hydrogen-bond donor and that might be a reason for the high activity of the compound, whereas, absence of hydrogen-bond donor group at the same position lead to a 5-fold decrease in activity of inactive compound (**85**; magenta-colored; pIC_{50} 6.51). Position 5 of pyridine ring can tolerate large heteroatom-containing substitutions and charged substitutions, as corroborated earlier [41]. This indicates that there might be some hydrophilic residues in active site that can interact with polar functional groups substituted on position 5 of pyridine ring leading to an increase in potency of these compounds.

Red-colored cubes near the phenyl ring attached to 4th position of imidazole ring in Fig. 4(B) indicate unfavorable region for hydrogen-bond donor groups. **16** (magenta-colored; activity 5.72) in Fig. 4(B) contains polar groups, specifically, hydrogen bond donor groups, on 4th position of imidazole ring, which are buried in the red-colored cubes; this might be a reason for lower potency of this compound. Whereas **4** (green-colored; activity 8.15) has hydrophobic groups instead of polar groups and this might have lead to higher activity of this compound. Similar comparison can be observed in **8** (activity 6.2), which does not have any substitution on 4th position of imidazole ring, while substitution of hydrogen-bond donor groups in **16** (5.72), **17** (5.53) and **18** (5.39) lead to a drastic decrease in activity of these compounds. Fig. 5(C) shows active and inactive compounds from benzimidazole series of compounds. **63** (magenta-colored; 5.72) contains an amino group at the para position of phenyl ring that is substituted on the 4th position of benzimidazole ring. This amino group is buried in unfavorable region for hydrogen-bond donor groups as indicated by the red-colored cubes. **50** (7.48) does not have any polar groups at the same position. The difference in IC_{50} values of both the compounds is more than 50-fold, thus indicating that hydrogen-bond donor groups might be unfavorable at this position. Visualization of effects with hydrogen-bond donor group regression coefficients gave similar results as experimental studies and indicates the importance of hydrogen-bond donor groups at specific points in these series of compounds. Experimental studies also reveal that some basic groups like pyridine (**59**; activity 6.57) or pyrimidine (**60**; activity 6.89) or 2-methoxy pyridine (**61**; activity 6.95) are tolerated at this position without perturbing the potency much. Blue-colored cubes can be observed near both the nitrogen atoms of the benzimidazole/imidazole ring indicating favorable tolerance of H-bond donor groups at those positions and also alluding to the fact that due to tautomerism, the cubes are observed at both the nitrogen atoms. Red-colored cubes beside the blue-colored cubes near the nitrogen atoms of the imidazole/benzimidazole ring indicate that H-bond donor groups are not favored at that position, while the SAR from experimental studies indicates that there might be steric limitations at that those positions [41]. This is clear from **32** (6.24)

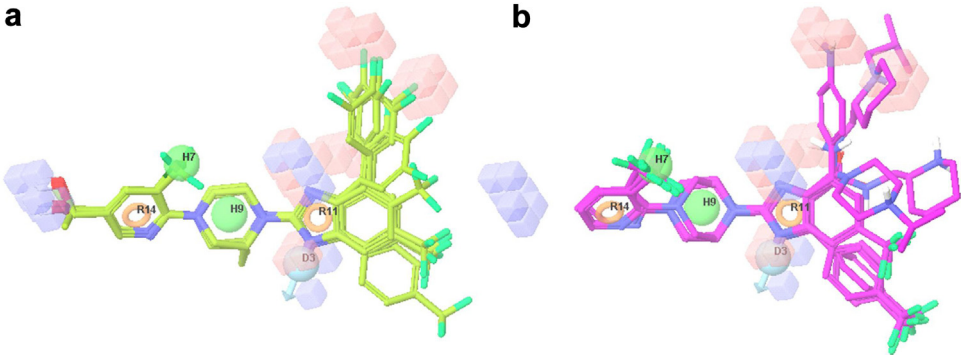

Fig. 5. Compounds that contributed positively and negatively to hydrogen-bond donor effects. Actives are green-colored; inactives are magenta-colored. (**a) 11** (9), **26** (8.85), **48** (9.22), **49** (8.59) and **90** (7.19) (**b) 15** (6.15), **16** (5.72), **17** (5.53), **20** (5.47) and **63** (5.72). The pIC_{50} values of the compounds are given in the parentheses. The cubes are as seen at a positive regression threshold of 0.006 and a negative regression threshold of −0.006. (For interpretation of the references to color in this figure legend, the reader is referred to the web version of the article.)

and **33** (5.19) that have a benzyl group substituted on each nitrogen.

The occurrence of favorable regions for hydrogen-bond donor groups at specific points on the scaffold is due to the presence of hydrogen-bond donor groups at those positions in some of the active compounds and absence of the groups in less active compounds. These active compounds mostly have a methanol group at the 5th position of pyridine ring. Fig. 5(A) shows some active compounds, with their pIC_{50} values, positively contributing to this favorable region. Fig. 5(B) shows compounds negatively contributing to H-bond donor region. Most of these compounds have H-bond donor groups such as amine, aniline or piperidine variously substituted at the 4th position of imidazole/benzimidazole ring.

3.5.2. Analysis of hydrophobic effects

Hydrophobic effects are visualized at a positive and a negative regression coefficient threshold of 0.035 and −0.035, respectively, depicted in Fig. 6 showing actives and inactives with hydrophobic effects. Blue-colored cubes near the 4th position of the imidazole ring indicate the importance of hydrophobic group at that position and the absence of hydrophobic groups at this position might lead to a decrease in activity. As shown in Fig. 6(A), **8** (magenta-colored), with an activity of 6.2, has a methyl, which is not a large hydrophobic group, substituted on the 4th position of imidazole ring; substitution of a trifluoro-phenyl group in place of methyl group leads to **4** (green-colored) having an activity of 8.15, thus indicating the presence of a hydrophobic pocket and the importance of fairly large hydrophobic groups on the ligand at that position. Removal of the methyl group leads to a loss of activity as observed in **12** (6.06). Addition of various hydrophobic groups at the 4th position of imidazole ring and the consequent improvement in activity of the compounds can be observed by considering **1** (phenyl; 6.97), **3** (4-CF_3-phenyl; 6.24), **5** (3,5-difluoro-phenyl; 7.46) and **13** (chloro; 6.8). Considering the trend in potency due to the size of the substituent, H < methyl < phenyl < 3,5-difluoro-phenyl < 3,4,5-trifluoro phenyl, it appears that activity tends to improve with increasing size of hydrophobic group substituent. The analysis of hydrophobic contours at the same position in benzimidazole series of compounds is shown in Fig. 6(B). The benzimidazole series of compounds align well with the imidazole series of compounds such that the same region of blue-colored cubes appears near to the 4th position of benzimidazole ring. As shown in the Figure, **50** (green-colored) has a 3,4,5-trifluoro phenyl substitution at the 4th position of benzimidazole ring and shows an activity of 7.48, while **20** (magenta-colored) has an amino group in that position and shows an activity of 5.47, indicating that absence of a hydrophobic group at this position in **20** might be a reason for its less activity, while presence of a hydrophobic group at the same position as in **50** might have lead to a sharp improvement in activity. The trend of improvement in activity with increasing size or hydrophobicity of the hydrophobic substituent again indicates the presence of a fairly large hydrophobic pocket near the 4th position of benzimidazole ring: **70** (CF_3; 6.49) < **55** (phenyl; 6.85) < **54** (4-CF_3-phenyl; 7.29) < **57** (4-*t*-butyl-phenyl; 7.89). Presence of polar groups at the same position leads to a sharp decrease in activity: **19** (nitro; 5.78) and **63** (aniline; 5.72). Thus, as indicated by hydrophobic effects, this region is highly favorable for larger hydrophobic groups in both imidazole and benzimidazole series of compounds and substitution of larger hydrophobic groups at this position might lead to increase in activity. This preference for hydrophobic groups at this position and decrease in activity due deletion or absence of hydrophobic groups at this position has been corroborated in experimental studies [41,42].

A few blue-colored cubes near the piperazine ring show importance of hydrophobic groups at this position. As shown in Fig. 6(C), the difference between **9** (magenta-colored) and **10** (green-colored) is an R-methyl group on the piperazine ring of **10**, but the activity difference is almost 4-fold. Compound **9**, without the methyl group at this position has an activity of 7.05 while **10** with the methyl on piperazine ring has an activity of 7.59. Fig. 6(D) shows similar differences in two compounds of the benzimidazole series: **30** does not have any substitution on piperazine ring and its activity is 6.96, while **74** has a R-methyl substitution on the piperazine ring and its activity is 7.32. However, substitution of R-ethyl or R-propyl groups at the same position on the piperazine ring in **75** and **76** led to a decrease in activity to 6.19 and 5.49, respectively. This indicates that the R-methyl group on piperazine ring is favorable for activity in both the series of compounds, as corroborated by experimental studies that concluded that R-methyl seems to be preferred to S-methyl [41]. From the analysis of regression coefficients with hydrophobic effects it is clear that the two regions identified above are favorable for placement of hydrophobic groups. Hydrophobic groups at 4th position of imidazole/benzimidazole ring are important, as indicated by the sharp drop in activity for compounds lacking larger hydrophobic groups at that position. The relative importance of both the regions—4th position on the imidazole/benzimidazole ring and 2nd position with R-configuration on the piperazine ring—is evident by the number and density of cubes at each position at the given threshold of regression coefficients.

Substitutions at 5th position of the benzimidazole ring are detrimental for activity, exemplified by **30**, with no substitution at the 5th position on the benzimidazole ring, having an activity of 6.96 compared to **42**, with a 4-CF_3-phenyl at the same position,

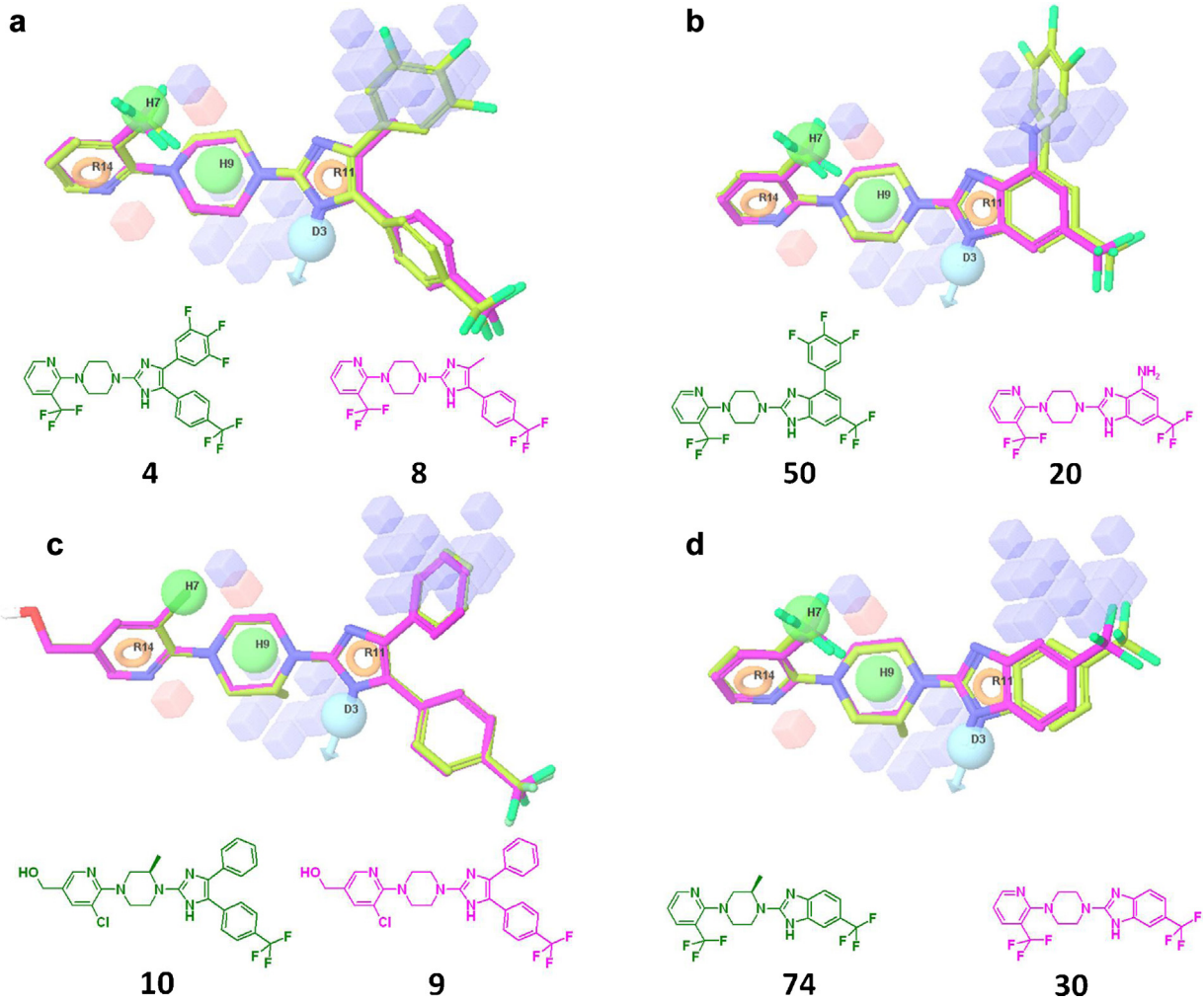

Fig. 6. Hydrophobic effects with active (green-colored stick models) and inactive (magenta-colored stick models) compounds of both series. (**a**) **4** (8.15) and **8** (6.20), (**b**) **50** (7.48) and **20** (5.47), (**c**) **10** (7.59) and **9** (7.05) and (**d**) **74** (7.32) and **30** (6.96). The pIC_{50} values of the compounds are given in the parentheses. The cubes are as seen at a positive regression threshold of 0.035 and a negative regression threshold of −0.035. (For interpretation of the references to color in this figure legend, the reader is referred to the web version of the article.)

having an activity of 5.08. Small hydrophobic substitutions at the 6th position of the benzimidazole ring are also important for enhancing the activity: **34**, **30** and **64** having a bromine (6.91), CF_3 (6.96) and a *t*-butyl (6.74), respectively are considerably more potent than compounds having a methyl (**65**; activity 5.47), fluoro (**66**; activity 5.4), chloro (**67**; activity 5.95) or a methyl ester group (**69**; activity 5.91). Compound **38** with a 3,4-difluoro-phenyl (5.94) and **68** with a cyano group (5.48) indicate that some spatial constraints might be present at that position restricting the size of hydrophobic groups that can be substituted.

Active compounds that give rise to strong and positive hydrophobic effects are shown in Fig. 7(A and B). Fig. 7(A) shows that the favorable region for hydrophobic groups near 4th position of imidazole/benzimidazole is contributed by highly active compounds mostly having trifluoro-phenyl or CF3-phenyl substitutions at that position. The IC_{50} values of those compounds are given in parentheses. Fig. 7(B) shows another favorable region for hydrophobic groups near the piperazine ring. Compounds with R-methyl substitution at this position are more active than compounds having no substitutions at the same position. Fig. 7(B) shows some of those compounds, containing R-methyl group that contributes to this favorable region for hydrophobic groups.

3.5.3. Analysis of negative ionic effects

Negative ionic effects are visualized at positive & negative coefficient thresholds of 0.0025 and −0.0025, respectively. Fig. 8 shows the negative ionic effects with two compounds from the benzimidazole series. Red-colored cubes near the 5th position of the terminal pyridine ring indicate unfavorable region for negative ionic groups. Compound **29** (magenta-colored) has a negative ionic group, carboxylate, buried in the unfavorable region, whereas **27** (green-colored) has a non-ionic group at the same place. Presence of an unfavorable negative ionic group might be a reason that **29** has an activity of 7.34, while **27** has an activity of 9.52. However, absence of any group or presence of non-polar group at the same position results in a slightly less potency as observed, respectively in **77** with an activity of 8.17 and **37**, having a bromide at that position, with an activity of 8.47. This indicates that absence of any negative ionic groups in that position may help in not adversely affecting the activity.

The dataset has only two compounds that carry a negative charge: **27** (COO^- group) and **19** (NOO^- group). Fig. 9 shows both the compounds and the red-colored cubes, indicating unfavorable region for negative ionic groups, near the 5th position of the terminal pyridine. For **19**, although the compound carries a negative charge, Phase does not assign a negative ionic feature to it as Phase

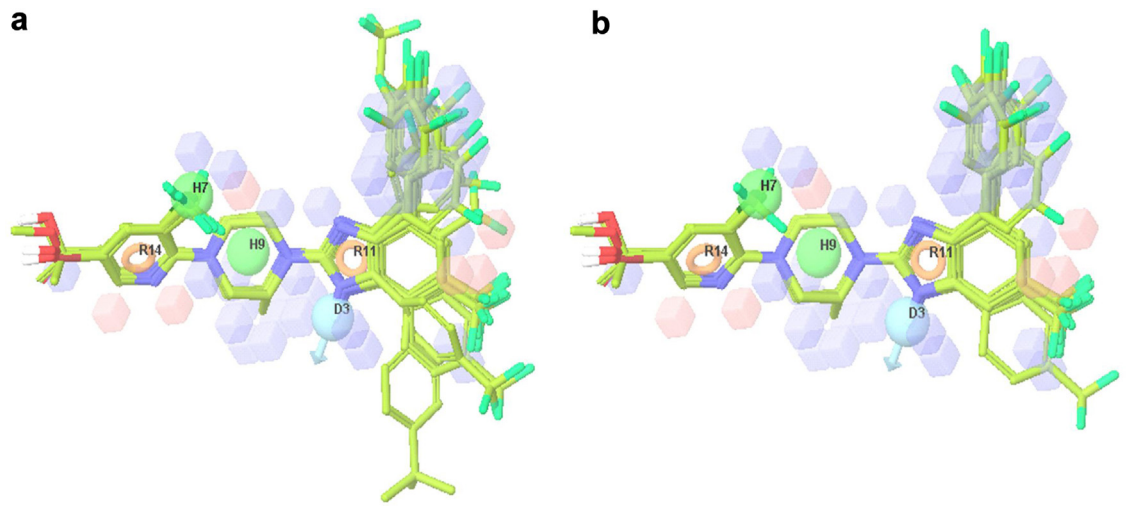

Fig. 7. Compounds that contributed positively to hydrophobic contours. (**a**) 4th position of imidazole/benzimidazole in compounds **4** (8.15), **11** (9), **26** (8.85), **27** (9.52), **37** (8.47), **41** (8.89), **48** (9.22), **49** (8.59) and **57** (7.89); (**b**) 2nd position on the piperazine ring in compounds **11** (9), **26** (8.85), **27** (9.52), **37** (8.47), **41** (8.89), **48** (9.22) and **49** (8.59). The pIC_{50} values of the compounds are given in the parentheses. The cubes are as seen at a positive regression threshold of 0.025 and a negative regression threshold of −0.025.

does not have a default feature definition for nitro group either as a H-bond acceptor or as a negative ionic group. Hence, although negative regression was observed for negative ionic groups at the 5th position of the terminal pyridine at the regression coefficient threshold of ±0.0025, no regression, positive or negative, was observed for negative ionic groups at the 5th position on the benzimidazole at the same threshold. But by considering structures of **19**, **50** and **30**, and relating them to their activities, it is clear that negative charge is not favorable at the 5th position of benzimidazole. **19**, with a nitro group carrying a formal negative charge, has an activity of 5.78, while **50** with a hydrophobic group (3,4,5-trifluorophenyl) at the same position has an activity of 7.48 and **30** with no substitution in that position has an activity of 6.96. These three compounds indicate that absence of a negative ionic group or any substitution at that position might help in not affecting the activity much, but presence of hydrophobic groups appears to enhance the activity as has already been described in the previous section.

3.5.4. *Analysis of positive ionic effects*

Positive ionic effects are visualized at positive and negative coefficient thresholds of 0.004 and −0.004, respectively. To understand the effect of positive ionic groups, effects due to positive ionic groups along with a few active and inactive compounds with substitutions projecting into the cubes are depicted in Fig. 10. Red-colored cubes above the imidazole ring indicate unfavorable region for positive ionic groups on the scaffold. **16** (magenta-colored),

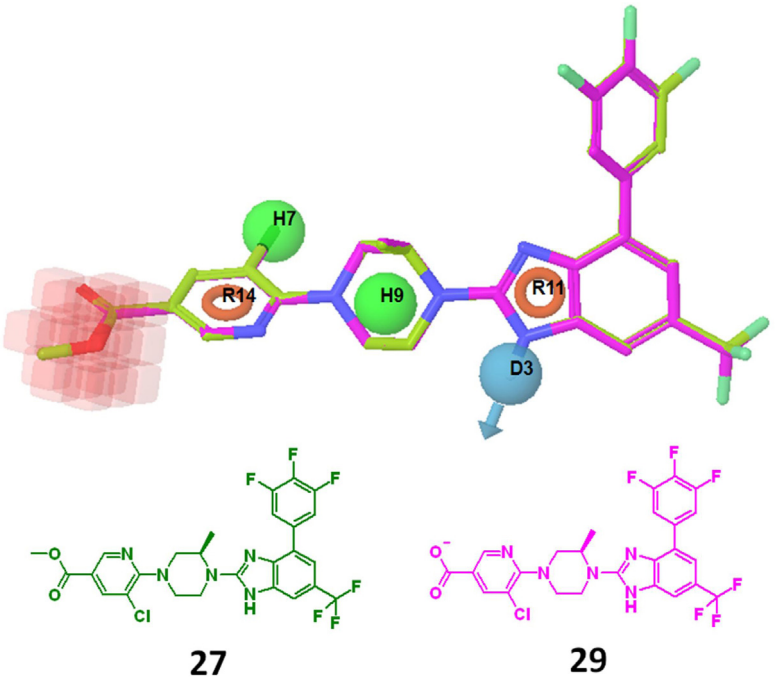

Fig. 8. Negative ionic effects with active (green-colored stick models) and inactive (magenta-colored stick models) compounds. The compounds with their pIC_{50} values in the parentheses are: **27** (9.52) and **29** (7.34). The cubes are as seen at a positive regression threshold of 0.0025 and a negative regression threshold of −0.0025. (For interpretation of the references to color in this figure legend, the reader is referred to the web version of the article.)

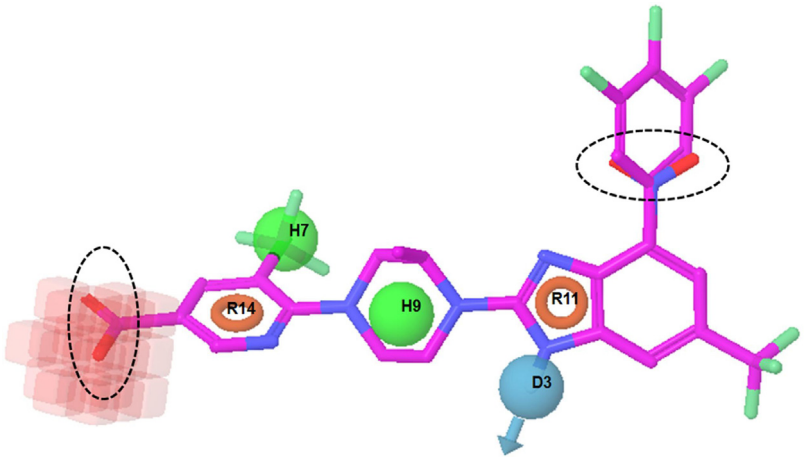

Fig. 9. Compounds that carry negative charges, shown by dashed circles, and contributed negatively to negative ionic effects, **29** (7.34) **19** (5.78). The pIC_{50} values of the compounds are given in the parentheses. The cubes are as seen at a positive regression threshold of 0.0025 and a negative regression threshold of −0.0025.

having an isobutyl group substituted on the nitrogen of piperidine that is attached to the 4th position of the imidazole ring through an amide shows the piperidine's nitrogen, that is protonated at a pH of 7.0, buried among the red-colored cubes. This compound has an activity of 5.72. **4** (green-colored) has a trifluoro-phenyl group substituted on the 4th position of the imidazole ring and has an activity of 8.15. This indicates that presence of a positive charge-bearing group that projects into the group of red-colored cubes above the imidazole ring tends to lower the activity, while hydrophobic groups in the same place appear to enhance activity. **12** does not have any substitution at the same position and it shows a moderate activity of 6.06. **17** and **18** also have positively charged groups, 2-piperidine and N-alkylated tetrahydro-pyrrole, respectively, at the same position and they are less active, with their activities as 5.53 and 5.39, respectively. Likewise **20** (5.47) has an amino group substituted at the same position and is less active. The effect of substitution of hydrophobic groups that mask the positive charge is exemplified by **63** (5.72), having a partial

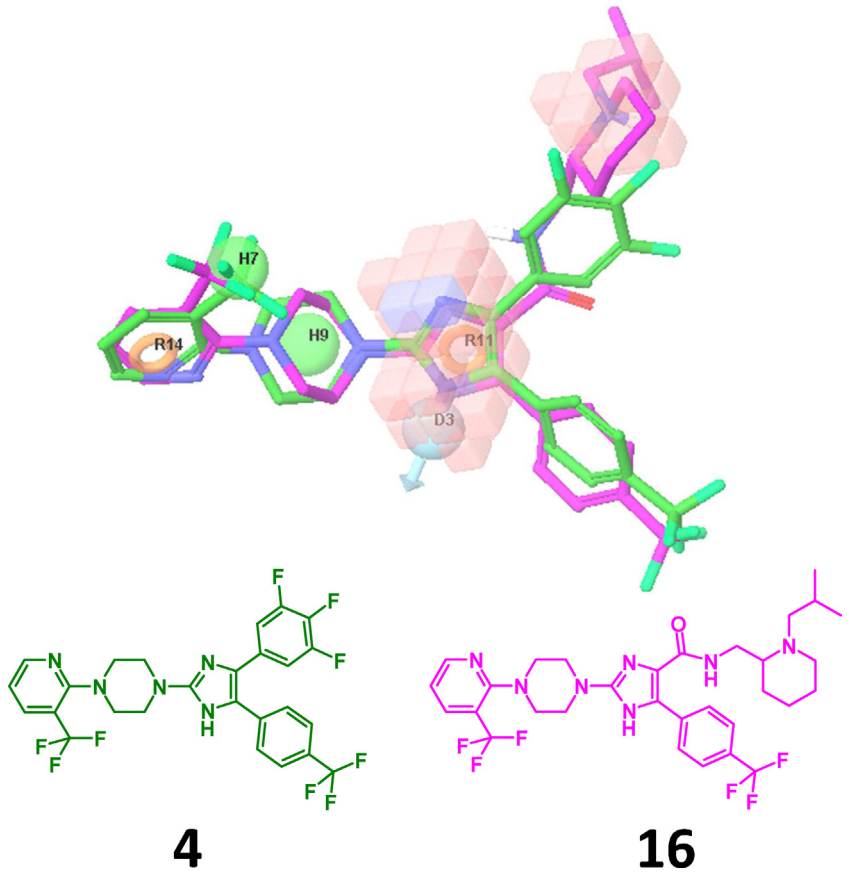

Fig. 10. Positive ionic effects with active (green-colored stick models) and inactive (magenta-colored stick models) compounds. The compounds with their pIC_{50} values in the parentheses are: **4** (8.15) and **16** (5.72). The cubes are as seen at a positive regression threshold of 0.004 and a negative regression threshold of −0.004. (For interpretation of the references to color in this figure legend, the reader is referred to the web version of the article.)

positive-charge-bearing aniline substituted on the 4th position of the benzimidazole ring and **39** (6.97), having a N,N-dimethyl substituted aniline. The difference in activity clearly indicates that while positively-charged groups do not seem to be beneficial for activity, non-polar or hydrophobic groups seem to be very effective in improving the activity. The group of red-colored cubes near both the nitrogen atoms of the imidazole ring that carry partial negative charge, indicate that positive ionic groups are unfavorable at that place of the scaffold. The small group of blue-colored cubes near one of the nitrogen atoms on the imidazole ring indicates a favorable region for positive ionic groups, but there are no examples of such compounds in the SAR to validate this observation. Moreover, tautomerism in the imidazole ring might erroneously indicate the blue-colored cubes at the incorrect nitrogen. This is substantiated by experimental studies that suggest that hydrogen-bond donors might be preferable at the nitrogen indicated by the hydrogen-bond donor pharmacophoric feature.

Visualization of effects due to negative and positive ionic groups revealed that the 4th position of imidazole/benzimidazole ring in both the series of compounds is unfavorable for negative and positive ionic groups on the scaffold. To reinforce this observation, both negative and positive ionic effects were combined and visualized, as shown in Fig. 11 to get an overall view of effect of polar groups on the activity in both series of compounds. The thresholds of both positive and negative regression were set to 0.004 and −0.004, respectively. Fig. 11 shows a pair of very active compounds, one each from imidazole (**11**; activity 9) and benzimidazole (**27**; activity 9.52) series, aligned and with their 3,4,5-trifluoro-phenyl substitutions on the 4th position of imidazole/benzimidazole ring projected into the red-colored cubes. The effects clearly show that polar groups are unfavorable at that position in the both series of compounds. Previously, the hydrophobic effects clearly showed that hydrophobic groups in the same position, near the 4th position of the imidazole, lead to a considerable improvement in activity. Experimental studies also reveal that hydrophobic groups at the 4th position of imidazole/benzimidazole ring, in both the series of compounds, are highly favorable for this region, thus confirming the inference from our analysis using the 3D-QSAR model.

While the thresholds of regression coefficients were set arbitrarily for visualization, a comparison of the thresholds (hydrogen-bond donor effects at ±0.006, hydrophobic effects at ±0.035, negative ionic effects at ±0.0025 and positive ionic effects at ±0.004) indicates that hydrophobic effects are dominant, reinforcing the inference that hydrophobic groups seem to have very beneficial effect on the activity of compounds in both the series. The favorable region for hydrophobic groups near the 4th position of imidazole and piperazine rings, shown by hydrophobic effects, and the unfavorable regions for polar groups near the 4th position imidazole and the piperazine, shown by the hydrogen-bond donor, negative ionic, and positive ionic effects, confirm that this binding pocket is fairly hydrophobic [52–54], probably lined with hydrophobic & aromatic amino acids. A TRPV1 antagonist, in general, should have a fairly hydrophobic core with hydrophobic substituents towards one end and polar substituents, preferably with hydrogen-bond donors, at the other end.

3.6. Alignment of other series of compounds to the pharmacophore model

Having built a unique and novel pharmacophore model leading to a validated 3D-QSAR model from the piperazinyl-aryl series, we wanted to test the general applicability of our pharmacophore model to other series of TRPV1 antagonists. If generally applicable, this model will be useful for generating novel and active chemotypes. Furthermore, this model would facilitate the identification of hot spots for potency improvement based on the alignment of compounds with potent compounds and their pharmacophoric features. We also explored the similarity in the binding modes for compounds of different diverse series by comparing the alignments of their 3D structures with the pharmacophore model. In order to explore the similarity in the binding modes (identified by low energy conformations) of compounds from different active series reported in the literature, we selected compounds from several representative series [2,21,23,34,55–60], including six clinical and six pre-clinical candidates (Table 3).

Fig. 12 shows the alignment of four compounds from four different series, along with **79** from the piperazinyl-aryl series for comparison, to the current pharmacophore hypothesis. It can be clearly observed that all the pharmacophore features are aligned well to the appropriate moieties of compounds of other series. Previous few studies revealed that an amide group is essential for compounds to be TRPV1 antagonists. This is represented by the H-bond donor feature (D3) represented by either the –NH of amide group or the –NH of imidazole group. All the aligned compounds have their H-bond donor group within the tolerance limit (1.0 Å) of the H-bond donor feature of the pharmacophore. The hydrophobic feature (H9) at the center of the pharmacophore model is represented by either the piperazine ring or an ethylene group. The other hydrophobic feature is represented by the CF_3 group in JNJ-17203212 and the chlorine group in BCTC which are well aligned to the feature. The ring aromatic feature (R14) is represented by the terminal phenyl or pyridyl ring. The other ring aromatic feature (R11), represented by the imidazole or the imidazole ring of the benzimidazole of the piperazinyl-aryl series of compounds, is represented by either a phenyl or a pyridyl ring in all the aligned compounds and aligns them within the tolerance limits of 1.5 Å.

Fig. 13 shows the alignment of three clinical and two preclinical compounds, all having different chemotype, to our pharmacophore hypothesis, including **79** from current dataset for comparison. It is seen here that all the pharmacophore features align well to similar moieties of compounds from other series. The H-bond donor is represented by –NH of the amide or urea, or a simple amine, except in AMG-628 in which the nitrogen of the pyrimidine ring is located near the H-bond donor feature. The H-bond donor moieties in SB-705498 (urea), MK-2295 (amine), JTS-653 (amide) and SB-782443 (amide) align very well with the H-bond donor feature of the pharmacophore model. The hydrophobic feature (H9) at the center of the pharmacophore model is represented by either a quinazoline ring, or a benz[1,4]oxazine ring or a pyrrolidine ring or a pyridine ring or a piperazine ring and these align well with the pharmacophore feature. The region of the TRPV1 active site represented by this feature appears to favor a lipophilic group represented either by a hydrophobic or an aromatic group. The ring aromatic feature (R14) is represented by the terminal phenyl or pyridyl ring, which appear to align with the feature well within its tolerance limit of 1.5 Å. The other hydrophobic feature (H7) is represented by a CF_3 group in MK-2295, a methyl group in AMG-628 and a chloro group in JTS-653, while it is unrepresented in SB-705498 and SB-782443. The other ring aromatic feature, R11, aligns well only with the pyrimidine group of AMG-628. Had the phenyl ring of benzimidazole been represented as a ring aromatic feature, then the phenyl ring of JTS-653 would have aligned well with it and the phenyl groups of SB-705498, MK-2295 and SB-782443 would have aligned within its tolerance limits. This region of the TRPV1 active site appears to be broad and favor lipophilic groups represented by the ring aromatic feature in the pharmacophore model as well as by the hydrophobic regression effects (see Fig. 7). Hence it is not surprising, that although all compounds have aromatic groups in this region, they do not exactly match the pharmacophore feature. Due to the diversity of groups aligning the hydrophobic feature H9, as well as the variety of aromatic groups placed near the aromatic feature R11, the alignment of all six compounds shown in Fig. 13.

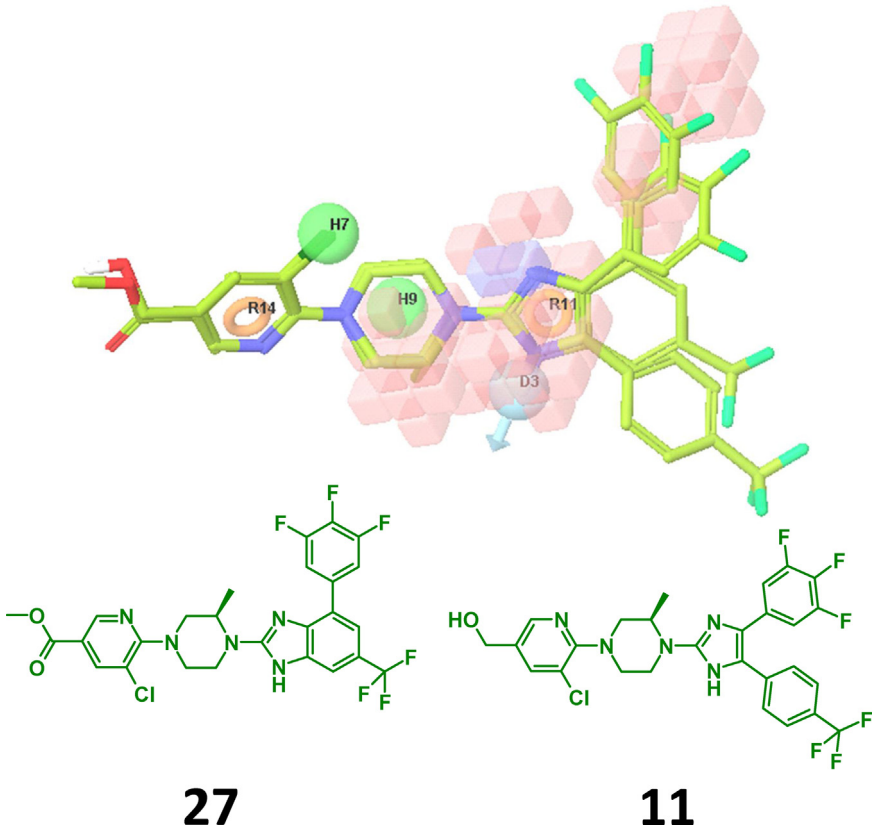

Fig. 11. Negative ionic and positive ionic effects combined, with two highly active compounds from both series: **27** (9.52) and **11** (9.0). The pIC_{50} values of the compounds are given in the parentheses. The cubes are as seen at a positive regression threshold of 0.004 and a negative regression threshold of −0.004.

Table 3
Details of known TRPV1 antagonists aligned to the pharmacophore model.

S. No	Compound	Fitness[a]	Compound status	Shape similarity[b]	Reference
1	SB-366791	1.53	Lead compound	0.53	[61]
2	JNJ-17203212	1.68	Lead compound	0.62	[62]
3	BCTC	1.67	Preclinical; not pursued further	0.62	[26]
4	AMG-9810	1.45	Lead compound	0.56	[24]
5	SB-705498	1.57	Phase II	0.48	[63–65]
6	AMG-628	0.84	Preclinical; not pursued further	0.66	[66–68]
7	MK-2295[c] (NGD-8243)	1.61	Phase II completed	0.55	[69,70]
8	JTS-653[c]	0.85	Phase II	0.61	[71,72]
9	SB-782443	0.88	Preclinical	0.59	[73,74]
10	M-68006[c]	0.50	Preclinical	0.49	[75,76]
11	SAR-115740[c]	1.01	Preclinical	0.64	[77]
12	AZD-1386[c]	1.02	Phase II (terminated)	0.45	[78]
13	ABT-102	0.47	Phase I	0.38	[79–82]
14	GRC-6211[c]	0.54	Phase (suspended)	0.52	[83,84]
15	**79**	2.64		0.90	[41]

[a] Using Phase. Fitness is a score that measures how well the compound's pharmacophore site points and vector features (acceptors, donors, and aromatic rings) align to the pharmacophore hypothesis and how well the compound's matching conformation superimposes with the reference ligand conformation. Higher the fitness value the better is the alignment.

[b] Using Phase_Shape. Compound's conformers are aligned to the query (reference compound **45**), and a similarity is computed based on overlapping hard-sphere volumes for the conformer showing the best match. Higher the similarity value the better is the match.

[c] Indicates that the compound structure given represents an example from a patent, illustrated since the identity of the lead molecule has not been disclosed.

appears imperfect, but individually all the compounds align very well and all of them represent most of the pharmacophore features in the pharmacophore model.

Alignment of five more compounds, three clinical – AZD-1386, ABT-102 and GRC-6211 – and two preclinical – M-68006 and SAR-115740 – from different series to our pharmacophore hypothesis revealed that all of them have the essential features illustrated by the pharmacophore model, but their mapping to the corresponding features in the pharmacophore model is not perfect. When these compounds are aligned to the pharmacophore model, at least one of their features does not map to the corresponding feature in the pharmacophore model. These compounds are quite diverse from the compounds of the dataset used in this modeling and this is clear from the alignment as the matching of their various groups with the corresponding features is not very ideal. Moreover, the compound structures given for AZD-1386, GRC-6211, M-68006 and SAR-115740, as well as for MK-2295 and JTS-653 in Fig. 13 represent examples from patents and may neither be the best nor the lead compounds of their respective series. Hence this fact also has to be borne in mind when alignment and fitness are being

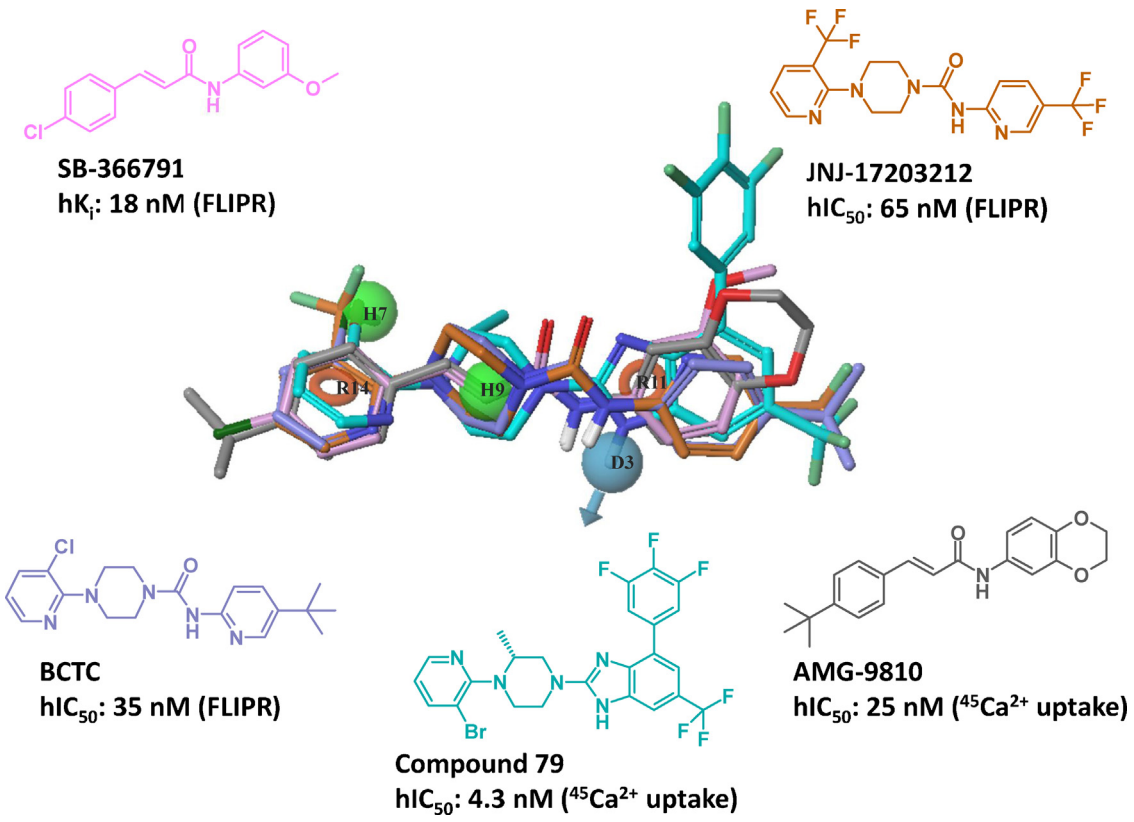

Fig. 12. Alignment of BCTC, AMG-9810 and compounds from two other series to the pharmacophore. Color codes: SB-366791 (pink), JNJ-17203212 (brown), BCTC (violet), **79** (cyan) and AMG-9810 (grey). (For interpretation of the references to color in this figure legend, the reader is referred to the web version of the article.)

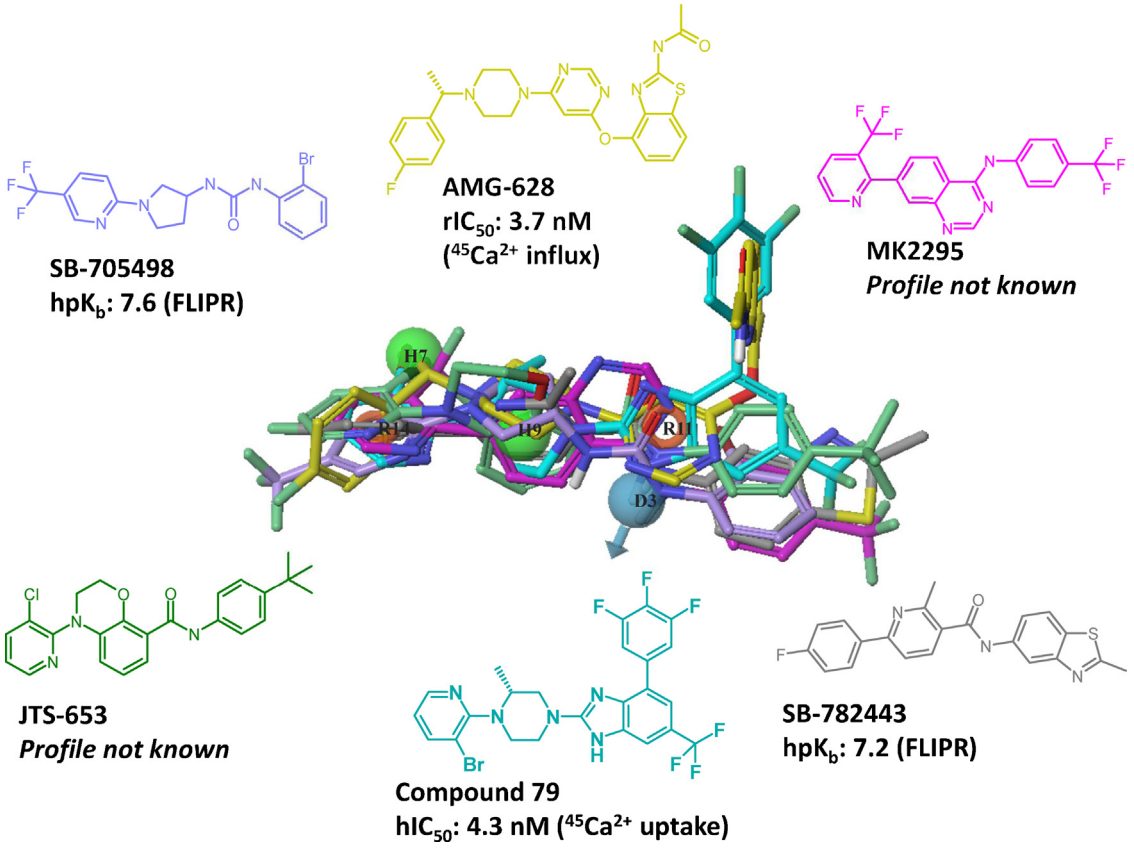

Fig. 13. Alignment of three clinical (SB-705498, MK2295 and JTS-653) and two preclinical (AMG-628 & SB-782443) candidates to the pharmacophore model. Color codes: SB-705498 (violet), AMG-628 (yellow), MK-2295 (pink), JTS-653 (green), **79** (cyan) and SB-782443 (grey). (For interpretation of the references to color in this figure legend, the reader is referred to the web version of the article.)

compared. We have observed that in case of some compounds, alternate alignments were also observed, but we have selected only those alignments in which most of the features are matching. From the alignments it is clear that a hydrogen-bond donor (D3), an aromatic ring (R14) and hydrophobic groups (H9) are essential features for antagonistic activity of the compounds. The table below (Table 3) shows the details of fitness values and shape similarity values of the compounds aligned to the pharmacophore model.

79 shows highest fitness and shape similarity as can be expected since the dataset is based on the same scaffold. The JNJ compound and BCTC, based on a similar scaffold (piperazine-1-carboxamide) as that of the dataset used in this experiment, show good fitness and shape similarity. SB-705498 and MK-2295 align very well with three and four features, respectively and hence show good fitness. SB-366791 and AMG-9810, based on a similar scaffold, align in a similar way to the pharmacophore model and show lower fitness and shape similarity compared to others. All the known compounds have a lower fitness and shape similarity compared to that of **79**, as they do not possess the ring aromatic feature on the right, represented by the imidazole/benzimidazole ring in the dataset compounds. Additionally, in SB-366791 and AMG-9810, the terminal phenyl ring on the left-hand side is slightly shifted (by less than 1.5 Å) with respect to the ring aromatic feature on the left of the pharmacophore model, as also reflected in the fitness values and shape similarity. SB-705498 has a low shape similarity despite having good fitness. In the aligned conformation of this compound, except for the urea group, all the three rings – phenyl, pyridyl and pyrrolidinyl – are co-planar and nearly orthogonal compared to rings in other compounds. ABT-102 is not represented by both the ring aromatic features and this is reflected in the low fitness and shape similarity scores for this compound. Except for **79**, the shape similarity values of all other compounds are very close, indicating that they all assume similar shapes when they bind [85]. Their shapes can be compared to those of **12** or **31** of the dataset, whose shape similarities are 0.62 and 0.60, respectively. The fitness & shape similarity values of the compounds cannot be correlated to their activities, as they are from different assays and experiments.

4. Conclusion

The goal of this study is to develop a model that facilitates the design of novel TRPV1 antagonists, for the treatment of pain. Towards the end, a novel and unique pharmacophore is presented here based on 3D-QSAR modeling of two closely related series of compounds, which is shown to have general applicability across several leads, clinical and pre-clinical candidates. The present study also explores the structure-activity relationships of piperazinyl-aryl series of TRPV1 antagonists using a pharmacophore-based 3D-QSAR model and offers a rationale for their observed activities. The 3D-QSAR model developed here, showed strong predictive correlations for test sets. The model was further validated by a *Y*-randomization study, which demonstrated the model to be non-random and unique. Thus the proposed model offers a rationale for observed structure–activity relationships of this series of compounds, which can be incorporated for designing novel antagonists of TRPV1. The 3D-QSAR effects using the regression coefficients revealed the importance of various pharmacophoric aspects at different positions of the aligned compounds and effect of various substitutions on the scaffold on the antagonistic activity. From this analysis it is clear that hydrophobic groups at the 4th position of the imidazole ring or the benzimidazole ring are important for activity, while substitutions at the nitrogen position of imidazole or benzimidazole ring lead to loss of activity. Hydrogen-bond donor groups at 5th position of the terminal pyridine ring appear to improve activity. The alignment of compounds from other series of TRPV1 antagonists, including three lead compounds, six clinical and five pre-clinical candidates to the pharmacophore hypothesis clearly emphasizes and validates the essential pharmacophoric features in all these antagonists.

5. Methods

5.1. Conformational analysis

LigPrep module [86] of Schrodinger was used to generate starting geometries of the compounds in the dataset. Protonation states were derived at a pH of 7.0 using *Epik* [87–89]. OPLS forcefield [90–92] was used for all geometry optimizations. MacroModel [93] was used for conformational analysis of all ligands. During conformation generation, potential energy calculation was carried out using the OPLS_2005 forcefield. An implicit solvent model [94] with extended cutoffs was used for energy calculations. Conformational search was carried out using Mixed Torsional/Low-mode sampling method [95–98] with extended torsional sampling option. Maximum number of steps used for conformation search was 2000, with 100 steps per rotatable bond. A maximum of 150 conformations per molecule were generated within an energy window of 10 kcal/mol. Redundant conformations were eliminated using an RMSD cutoff of 0.5 Å. The minimum and maximum distances for low mode were set to 3 Å and 6 Å, respectively.

5.2. Pharmacophore/3D-QSAR modeling

The pharmacophore hypothesis is generated using Phase QSAR module of Schrodinger, which employs a grid-based 3D-QSAR method [45,46], identifying the grid points closest to atoms in the molecules aligned to a selected reference compound, and these points are then used for generating 3D descriptors for different types of interactions, which are correlated to biological activities using a PLS approach.

All conformations, generated using MacroModel module of Schrodinger, were imported into the PHASE run. A pIC_{50} of 6.5 was set as the activity threshold to divide the dataset into an active pharm set of 39 compounds and an inactive pharm set of the remaining 38 compounds. The compounds of the active pharm set would be used to search for common pharmacophore hypotheses. After the pharmacophore sites were created for all compounds according to the default pharmacophore feature definitions, common pharmacophore hypotheses were searched with a criterion that the selected variant must match as least all the 39 actives. The pharmacophore hypotheses of all variants were scored by active and inactive compounds to identify a set of hypotheses that provide the best alignment of all chosen actives. This step provided all hypotheses with their scores, based on alignment of actives and inactives, to develop 3D-QSAR models.

Each common pharmacophore hypothesis yields an alignment of all compounds that is the input for QSAR modeling. For a given alignment, QSAR models are built by adding PLS factors until a maximum of $n/5$ PLS factors, where n is the number compounds in the training set. In this experiment 10 PLS factors were allowed. Thus many 3D-QSAR models will be generated in this step of the PHASE workflow. All these models are validated using various statistical methods. The built models are validated by an internal test set that is selected each time randomly from the Phase dataset of 77 compounds in the ratio 80:20, 80% comprising the training set (62 compounds) and 20% comprising the internal test set (15 compounds). The large number of models is filtered using the output

statistical measures of the internal test set to yield a much smaller set of models that can be tested using the external test set. The models are further validated using external test sets with known activities. Most of the models validated using the external test set were good in terms of the statistical parameters considered. The various validation measures considered as well as the correlation of SAR interpreted from the models with the SAR insights offered in the articles associated with the dataset together constituted a primary step to ensure that the model was robust enough. The main objective of this study was to build a pharmacophore model to assess its applicability to diverse series including the various clinical candidates and hence much focus was towards selecting a general and minimal pharmacophore model that shows most of the pharmacophoric features present in most of the TRPV1 antagonists reported thus far and that can align most of them. The model can then be used for virtual screening of databases to mine novel chemotypes that can potentially be developed into efficacious TRPV1 antagonists.

The dataset of 98 compounds was divided into the training set and external test set using many other methodologies apart from *k*-means clustering, like Jarvis-Patrick clustering [99], sphere exclusion [100], hierarchical clustering [101] and randomly, to check if the final models built from those sets were very different from each other. Pharmacophore hypotheses having more than and less than five features were also developed to check if slight changes in alignment can affect the QSAR models. Various 4-point and 5-point pharmacophore models and subsequent 3D-QSAR models built using different training and test sets gave very similar statistical metrics. For all the models developed, while the training set R^2 was between 0.90 and 0.98, the Q^2 for internal test set varied from 0.63 to 0.90 and the $R^2_{predicted}$ of the external test set varied from 0.60 to 0.78, indicating that the composition of sets did not have much effect on the models. These values are not much different from the values for the selected model. The model selection was done based on alignment of compounds and correlation of the SAR reported in the articles, from which the dataset was derived, with interpretation of SAR from the models. For the selected model, the average pair-wise compound similarities in all the datasets were fairly close: 0.31 for the training set, 0.35 for the internal test set and 0.29 for the external test set, using Daylight fingerprints as calculated by Schrodinger Canvas [102], followed by Tanimoto similarity calculation. The distribution of compounds over the ranges of activity, molecular weight, calculated log *P* (Alog *P*) [103] and polar surface area was similar, especially between the training set and the external test set. The frequency distribution charts are given in the supplementary information. An R-group analysis of all the three sets using CIMPL [44] revealed that the external test set had seven unique functional groups that were not represented in the training set: benzyl substitution in the 1st position of benzimidazole (**32**), secondary amines in the 4th and 5th positions of benzimidazole (**21** and **43**, respectively), ester (**89**) in the *ortho*, keto (**28**), carboxylate (**29**), and amino (**44**) in the *para*, and CF_3 (**82**) in the *meta* positions of the terminal pyridine. The internal test set had five unique functional groups that were not represented in the training set: morpholine (**47**) and alicyclic ring (**53**; cyclohexyl) in the 4th position of benzimidazole, ester (**27**) and a reverse amide (**45**) in the *para* position of the terminal pyridine and a pyrimidine (**98**) attached to the piperazine. Though differences exist between the three sets in the form of functional groups in various positions, they are addressed in the training set by the common pharmacophore groups in the same positions. One exception is **89**, that differs from most other compounds in having an ester group in the *ortho* position of the terminal pyridine, while most others have a CF_3 group. This appeared as an outlier as mentioned earlier in section 3.3.

5.3. Y-randomization study

Some QSAR models may show chance correlations. When selecting descriptors that are of relevance to modeling activity or any property of interest, it is possible that some descriptors may lead to high chance correlations, though they may not be important fundamentally. *Y*-randomization method is very useful in these cases to eliminate such chance correlations. This is done by randomizing the activity value, that is, the independent variable, *Y*, in the QSAR equation, of the training set compounds without changing values of descriptors, followed by building and testing the model using the external test set compounds. This process is repeated a number of times and the $R^2_{predicted}$ values of all the models are compared with that of the original model. A clear discrimination between the $R^2_{predicted}$ values of the randomized models and the original model indicates that the descriptors do not enhance correlations by chance and rules out the possibility that the original model is by a chance correlation [50,51]. In this study, 100 models were generated by scrambling the activity data among the dataset compounds, and tested to rule out any chance correlation. The plot given in figure S1 of supplementary information gives the results for these 100 models (the blue-colored diamonds) as well as the original model (magenta-colored diamond). It can be seen clearly in the plot that the original model appears well separated from the models generated by randomizing activity data, thus validating the original model as not a case of chance correlation.

Appendix A. Supplementary data

Supplementary data associated with this article can be found, in the online version, at http://dx.doi.org/10.1016/j.jmgm.2013.08.014.

References

[1] R. Padinjat, S. Andrews, TRP channels at a glance, J. Cell Sci. 117 (2004) 5707–5709.
[2] M.M. Moran, M.A. McAlexander, T. Bíró, A. Szallasi, Transient receptor potential channels as therapeutic targets, Nat. Rev. Drug Disc. 10 (2011) 601–620.
[3] M.A. Schumacher, TRP channels in pain and inflammation: therapeutic opportunities, Pain Pract. 10 (2010) 185–200.
[4] A. Messeguer, R. Planells-Cases, A. Ferrer-Montiel, Physiology and pharmacology of the vanilloid receptor, Curr. Neuropharmacol. 4 (2006) 1–15.
[5] A. Jara-Oseguera, S.A. Simon, T. Rosenbaum, TRPV1: ON THE ROAD TO PAIN RELIEF, Curr. Mol. Pharmacol. 1 (2008) 255–269.
[6] M. Trevisani, A. Szallasi, Targeting TRPV1-challenges and issues in pain management, Open Drug Discov. J. 2 (2010) 37–49.
[7] B. Nilius, G. Owsianik, T. Voets, J.A. Peters, Transient receptor potential cation channels in disease, Physiol. Rev. 87 (2007) 165–217.
[8] P.M. Zygmunt, J. Petersson, D.A. Andersson, J. Chuang, M. Sorgard, V. DiMarzo, D. Julius, E.D. Hogestatt, Vanilloid receptors on sensory nerves mediate the vasodilator action of anandamide, Nature 400 (1999) 452–457.
[9] M. Tognetto, S. Amadesi, S. Harrison, C. Creminon, M. Trevisani, M. Carreras, M. Matera, P. Gepetti, A. Bianchi, Anandamide excites central terminals of dorsal root ganglion neurons via vanilloid receptor-1 activation, Neuroscience 21 (2001) 1104–1109.
[10] S.W. Hwang, H. Cho, J. Kwak, S.Y. Lee, C.J. Kang, J. Jung, S. Cho, K.H. Min, Y.G. Suh, D. Kim, U. Oh, Direct activation of capsaicin receptors by products of lipoxygenases: endogenous capsaicin-like substances, Proc. Natl. Acad. Sci. USA 97 (2000) 6155–6160.
[11] C.M. Flores, M.R. Vasko, The deorphanization of TRPV1 and the emergence of octadecadienoids as a new class of lipid transmitters, Mol. Interv. 10 (2010) 137–140.
[12] A.M. Patwardhan, P.E. Scotland, A.N. Akopian, K.M. Hargreaves, Activation of TRPV1 in the spinal cord by oxidized linoleic acid metabolites contributes to inflammatory hyperalgesia, Proc. Natl. Acad. Sci. USA 106 (2009) 18820–18824.
[13] A.M. Patwardhan, A.N. Akopian, N.B. Ruparel, A. Diogenes, S.T. Weintraub, C. Uhlson, R.C. Murphy, K.M. Hargreaves, Heat generates oxidized linoleic acid metabolites that activate TRPV1 and produce pain in rodents, J. Clin. Invest. 120 (2010) 1617–1626.
[14] M.J. Caterina, M.A. Schumacher, M. Tominaga, T.A. Rosen, J.D. Levine, D. Julius, The capsaicin receptor: a heat-activated ion channel in the pain pathway, Nature 389 (1997) 816–824.

[15] M.J. Caterina, T.A. Rosen, M. Tominaga, A.J. Brake, D. Julius, Capsaicin-receptor homologue with a high threshold for noxious heat, Nature 398 (1999) 436–441.
[16] M. Tominaga, M.J. Caterina, A.B. Malmberg, T.A. Rosen, H. Gilbert, K. Skinner, B.E. Raumann, A.I. Basbaum, D. Julius, The cloned capsaicin receptor integrates multiple pain-producing stimuli, Neuron 21 (1998) 531–543.
[17] A. Szallasi, P.M. Blumberg, Vanilloid (Capsaicin) receptors and mechanisms, Pharmacol. Rev. 51 (1999) 159–212.
[18] L.A. Roberts, M. Connor, TRPV1 antagonists as a potential treatment for hyperalgesia Recent Pat, CNS Drug Discov. 1 (2006) 65–76.
[19] S.E. Jordt, D. Julius, Molecular basis for species-specific sensitivity to "hot" chili peppers, Cell 108 (2002) 421–430.
[20] M.Z. Chou, T. Mtui, Y.D. Gao, M. Kohler, R.E. Middleton, Resiniferatoxin binds to the capsaicin receptor (TRPV1) near the extracellular side of the S4 transmembrane domain, Biochemistry 43 (2004) 2501–2511.
[21] A. Szallasi, D.N. Cortright, C.A. Blum, S.R. Eid, The vanilloid receptor TRPV1: 10 years from channel cloning to antagonist proof-of-concept, Nat. Rev. Drug Discov. 6 (2007) 357–372.
[22] S.G. Lehto, R. Tamir, H. Deng, L. Klionsky, R. Kuang, A. Le, D. Lee, J.C. Louis, E. Magal, B.H. Manning, J. Rubino, S. Surapaneni, N. Tamayo, T. Wang, J. Wang, J. Wang, W. Wang, B. Youngblood, M. Zhang, D. Zhu, M.H. Norman, N.R. Gavva, Antihyperalgesic effects of (*R,E*)-*N*-(2-hydroxy-23-dihydro-1H-inden-4-yl)-3-(2-(piperidin-1-yl)-4-(trifluoromethyl)phenyl)-acrylamide (AMG8562), a novel transient receptor potential vanilloid type 1 modulator that does not cause hyperthermia in rats, J. Pharmacol. Exp. Ther. 326 (2008) 218–229.
[23] G.Y. Wong, N.R. Gavva, Therapeutic potential of vanilloid receptor TRPV1 agonists and antagonists as analgesics: recent advances and setbacks, Brain Res. Rev. 60 (2009) 267–277.
[24] N.R. Gavva, R. Tamir, Y. Qu, L. Klionsky, T.J. Zhang, D. Immke, J. Wang, D. Zhu, T.W. Vanderah, F. Porreca, E.M. Doherty, M.H. Norman, K.D. Wild, A.W. Bannon, J.C. Louis, J.J. Treanor, AMG 9810 [(*E*)-3-(4-*t*-butylphenyl)-*N*-(23-dihydrobenzo[b][1,4] dioxin-6-yl)acrylamide], a novel vanilloid receptor 1 (TRPV1) antagonist with antihyperalgesic properties, J. Pharmacol. Exp. Ther. 313 (2005) 474–484.
[25] Q. Sun, L. Tafesse, K. Islam, X. Zhou, S.F. Victory, C. Zhang, M. Hachicha, L.A. Schmid, A. Patel, Y. Rotshteyn, K.J. Valenzano, D.J. Kyle, 4-(2-Pyridyl)piperazine-1-carboxamides: potent vanilloid receptor 1 antagonists, Bioorg. Med. Chem. Lett. 13 (2003) 3611–3616.
[26] K.J. Valenzano, E.R. Grant, G. Wu, M. Hachicha, L. Schmid, L. Tafesse, Q. Sun, Y. Rotshteyn, J. Francis, J. Limberis, S. Malik, E.R. Whittemore, D. Hodges, *N*-(4-Tertiarybutylphenyl)-4-(3-chloropyridin-2-yl)tetrahydropyrazine-1(2*H*)-carbox-amide (BCTC), a novel, orally effective vanilloid receptor 1 antagonist with analgesic properties: I. In vitro characterization and pharmacokinetic properties, J. Pharmacol. Exp. Ther. 306 (2003) 377–386.
[27] V.N. Viswanadhan, Y. Sun, M.H. Norman, Three-dimensional quantitative structure-activity relationships and activity predictions of human TRPV1 channel antagonists: comparative molecular field analysis and comparative molecular similarity index analysis of cinnamides, J. Med. Chem. 50 (2007) 5608–5619.
[28] R.D. Cramer, D.E. Patterson, J.D. Bunce, Comparative molecular field analysis (CoMFA). 1. Effect of shape on binding of steroids to carrier proteins, J. Am. Chem. Soc. 110 (1988) 5959–5967.
[29] G. Klebe, U. Abraham, T. Mietzner, Molecular similarity indices in a comparative analysis (CoMSIA) of drug molecules to correlate and predict their biological activity, J. Med. Chem. 37 (1994) 4130–4146.
[30] T. Taskin, F. Sevin, QSAR approach to correlate TRPV1 antagonist activity for a series of heteroaromatic urea, QSAR Comb. Sci. 28 (2009) 1098–1111.
[31] W.S. Cheung, R.R. Calvo, B.A. Tounge, S.P. Zhang, D.R. Stone, M.R. Brandt, T. Hutchinson, C.M. Flores, M.R. Player, Discovery of piperidine carboxamide TRPV1 antagonists, Bioorg. Med. Chem. Lett. 18 (2008) 4569–4572.
[32] K.H. Kim, 3-D-QSAR analysis of N-(3-acyloxy-2-benzylpropyl)-N′-dihydroxytetrahydrobenzazepine and tetrahydroisoquinoline and N-(3-acyloxy-2-benzylpropyl)-N-(4-hydroxy-3-methoxybenzyl) thioureas analogues as potent vanilloid receptor ligands, Bioorg. Med. Chem. 10 (2002) 1367–1372.
[33] Phase, version 2.0.212, 2005, Schrodinger LLC, New York, NY 10036-4041.
[34] P.R. Kym, M.E. Kort, C.W. Hutchins, Analgesic potential of TRPV1 antagonists, Biochem. Pharmacol. 78 (2009) 211–216.
[35] L. Tafesse, Q. Sun, L. Schmid, K.J. Valenzano, Y. Rotshteyn, X. Su, D.J. Kyle, Synthesis and evaluation of pyridazinylpiperazines as vanilloid receptor 1 antagonists, Bioorg. Med. Chem. Lett. 14 (2004) 5513–5519.
[36] R. Bakthavatchalam, Capsaicin receptor ligands, WO 02008221-A2, 2002.
[37] S. Dax, A. Dublin, M. Jetter, N. Nasser, C. Shah, D. Swanson, N.I. Carruthers, Vanilloid receptor antagonists: structure-activity relationships via parallel and targeted synthesis, Drugs Fut. 27 (Suppl. A) (2002) 93.
[38] T. Yura, M. Mogi, Y. Ikegami, T. Masuda, T. Kokubo, K. Urbahns, N. Yoshida, M. Marumo, M. Shiroo, M. Tajimi, K. Takeshita, T. Moriwaki, Y. Tsukumi, Piperazinecarboxamide derivative, JP 2003192673-A2, 2003.
[39] H.K. Rami, M. Thompson, G.J. Macdonald, S.M. Westaway, D.J. Mitchell, Vanilloid receptor modulators, WO 03068749-A1, 2003.
[40] C.H. Lee, E.K. Bayburt, S. Didomenico. Jr, I. Drizin, A.R. Gomtsyan, J.R. Koenig, R.J. Perner, R.G. Schmidt, S.C. Turner, T.K. White, G.Z. Zheng, Fused azabicyclic compounds that inhibit vanilloid receptor subtype 1 (VR1) receptor, WO 03070247, 2003.
[41] V.I. Ognyanov, C. Balan, A.W. Bannon, Y. Bo, C. Dominguez, C. Fotsch, V.K. Gore, L. Klionsky, V.V. Ma, Y.X. Qian, R. Tamir, X. Wang, N. Xi, S. Xu, D. Zhu, N.R. Gavva, J.J. Treanor, M.H. Norman, Design of potent, orally available antagonists of the transient receptor potential vanilloid 1Structure-activity relationships of 2-Piperazin-1-yl-1H-benzimidazoles, J. Med. Chem. 49 (2006) 3719–3742.
[42] V.K. Gore, V.V. Ma, R. Tamir, N.R. Gavva, J.J. Treanor, M.H. Norman, Structure-activity relationship (SAR) investigations of substituted imidazole analogs as TRPV1 antagonists, Bioorg. Med. Chem. Lett. 17 (2007) 5825–5830.
[43] J. Ghosh, A. Liu, K-Means, in: X. Wu, V. Kumar (Eds.), The Top Ten Algorithms in Data Mining (Chapman & Hall/CRC Data Mining and Knowledge Discovery Series), Chapman & Hall/CRC, Taylor & Francis Group, Boca Raton, FL, 2009.
[44] CIMPL, 2008, Cimplsoft Inc, Newbury Park, CA, www.cimplsoft.com
[45] S.L. Dixon, A.M. Smondyrev, E.H. Knoll, S.N. Rao, D.E. Shaw, R.A. Friesner, PHASE: a new engine for pharmacophore perception 3D QSAR model development, and 3d database screening. 1. Methodology and preliminary results, J. Comput. Aided Mol. Des. 20 (2006) 647–671.
[46] S.L. Dixon, A.M. Smondyrev, S.N. Rao, PHASE: a novel approach to pharmacophore modeling and 3D database searching, Chem. Biol. Drug Des. 67 (2006) 370–372.
[47] A.K. Ghose, G.M. Crippen, G.R. Revankar, P.A. McKernan, D.F. Smee, R.K. Robins, Analysis of the in vitro antiviral activity of certain ribonucleosides against parainfluenza virus using a novel computer aided receptor modeling procedure, J. Med. Chem. 32 (1989) 746–756.
[48] G.M. Crippen, Validation of EGSITE2, a mixed integer program for deducing objective site models from experimental binding data, J Med. Chem. 40 (1997) 3161–3172.
[49] G.M. Crippen, S.A. Wildman, Quantitative structure-activity relationships (QSAR), in: A.K. Ghose, V.N. Viswanadhan (Eds.), A Review of 3D-QSAR. Combinatorial Library Design and Evaluation, Marcel Dekker, Inc., New York, NY, 2001, pp. 131–156.
[50] C. Rücker, G. Rücker, M. Meringer, y-Randomization and its variants in QSPR/QSAR, J. Chem. Inf. Model. 47 (2007) 2345–2357.
[51] A. Tropsha, P. Gramatica, V.K. Gombar, The importance of being earnest: validation is the absolute essential for successful application and interpretation of QSPR models, QSAR Comb. Sci. 22 (2003) 69–77.
[52] K. Urbahns, T. Yura, M. Mogi, M. Tajimi, H. Fujishima, T. Masuda, N. Yoshida, T. Moriwaki, T.B. Lowinger, H. Meier, F. Chan, D. Madge, J.B. Gupta, Naphthol derivatives as TRPV1 inhibitors for the treatment of urinary incontinence, Bioorg. Med. Chem. Lett. 21 (2011) 3354–3357.
[53] H.G. Park, M.K. Park, J.Y. Choi, S.H. Choi, J. Lee, B.S. Park, M.G. Kim, Y.G. Suh, H. Cho, U. Oh, J. Lee, H.D. Kim, Y.H. Park, H.J. Koh, K.M. Lim, J.H. Moh, S.S. Jew, Synthesis of *N,N′,N″*-trisubstituted thiourea derivatives and their antagonist effect on the vanilloid receptor, Bioorg. Med. Chem. Lett. 13 (2003) 601–604.
[54] H. Ryu, M.K. Jin, S.Y. Kim, H.K. Choi, S.U. Kang, D.W. Kang, J. Lee, L.V. Pearce, V.A. Pavlyukovets, M.A. Morgan, R. Tran, A. Toth, D.J. Lundberg, P.M. Blumberg, Stereospecific high-affinity TRPV1 antagonists: chiral *N*-(2-benzyl-3-pivaloyloxypropyl) 2-[4-(methylsulfonylamino)phenyl]propionamide analogues, J. Med. Chem. 51 (2008) 57–67.
[55] E.A. Voight, M.E. Kort, Transient receptor potential vanilloid-1 antagonists: a survey of recent patent literature, Exp. Opin. Ther. Patents 20 (2010) 1107–1122.
[56] N. Khairatkar-Joshi, A. Szallasi, TRPV1 antagonists: the challenges for therapeutic targeting, Trends Mol. Med. 15 (2009) 14–22.
[57] M.J. Gunthorpe, B.A. Chizh, Clinical development of TRPV1 antagonists: targeting a pivotal point in the pain pathway, Drug Discov. Today 14 (2009) 56–67.
[58] A. Patapoutian, S. Tate, C.J. Woolf, Transient receptor potential channels: targeting pain at the source, Nat. Rev. Drug Discov. 8 (2009) 55–68.
[59] M. Trevisani, A. Szallasi, Targeting TRPV1: challenges and issues in pain management, Open Drug Discov. J. 2 (2010) 37–49.
[60] J.J. Adcock, TRPV1 receptors in sensitisation of cough and pain reflexes, Pulm. Pharmacol. Ther. 22 (2009) 65–70.
[61] M.J. Gunthorpe, H.K. Rami, J.C. Jerman, D. Smart, C.H. Gill, E.M. Soffin, S. Luis Hannan, S.C. Lappin, J. Egerton, G.D. Smith, A. Worby, L. Howett, D. Owen, S. Nasir, C.H. Davies, M. Thompson, P.A. Wyman, A.D. Randall, J.B. Davis, Identification and characterisation of SB-366791, a potent and selective vanilloid receptor (VR1/TRPV1) antagonist, Neuropharmacology 46 (2004) 133–149 (Erratum in: Neuropharmacology 46(2004) 905).
[62] D.M. Swanson, A.E. Dubin, C. Shah, N. Nasser, L. Chang, S.L. Dax, M. Jetter, J.G. Breitenbucher, C. Liu, C. Mazur, B. Lord, L. Gonzales, K. Hoey, M. Rizzolio, M. Bogenstaetter, E.E. Codd, D.H. Lee, S.P. Zhang, S.R. Chaplan, N.I. Carruthers, Identification and biological evaluation of 4-(3-trifluoromethylpyridin-2-yl)piperazine-1-carboxylic acid (5-trifluoromethylpyridin-2-yl)amide, a high affinity TRPV1 (VR1) vanilloid receptor antagonist, J. Med. Chem. 48 (2005) 1857–1872.
[63] H.K. Rami, M. Thompson, G. Stemp, S. Fell, J.C. Jerman, A.J. Stevens, D. Smart, B. Sargent, D. Sanderson, A.D. Randall, M.J. Gunthorpe, J.B. Davis, Discovery of SB-705498: a potent, selective and orally bioavailable TRPV1 antagonist suitable for clinical development, Bioorg. Med. Chem. Lett. 16 (2006) 3287–3291.
[64] B.A. Chizh, M.B. O'Donnell, A. Napolitano, J. Wang, A.C. Brooke, M.C. Aylott, J.N. Bullman, E.J. Gray, R.Y. Lai, P.M. Williams, J.M. Appleby, The effects of the TRPV1 antagonist SB-705498 on TRPV1 receptor-mediated activity and inflammatory hyperalgesia in humans, Pain 132 (2007) 132–141.
[65] M.J. Gunthorpe, S.L. Hannan, D. Smart, J.C. Jerman, S. Arpino, G.D. Smith, S. Brough, J. Wright, J. Egerton, S.C. Lappin, V.A. Holland, K. Winborn, M. Thompson, H.K. Rami, A. Randall, J.B. Davis, Characterization of SB-705498, a potent and selective vanilloid receptor-1 (VR1/TRPV1) antagonist that inhibits the

capsaicin-, acid-, and heat-mediated activation of the receptor, J. Pharmacol. Exp. Ther. 321 (2007) 1183–1192.
[66] H.L. Wang, J. Katon, C. Balan, A.W. Bannon, C. Bernard, E.M. Doherty, C. Dominguez, N.R. Gavva, V. Gore, V. Ma, N. Nishimura, S. Surapaneni, P. Tang, R. Tamir, O. Thiel, J.J.S. Treanor, M.H. Norman, Novel vanilloid receptor-1 antagonists: 3. The identification of a second-generation clinical candidate with improved physicochemical and pharmacokinetic properties, J. Med. Chem. 50 (2007) 3528–3539.
[67] H.L. Wang, C. Balan, E.M. Doherty, J.R. Falsey, V.K. Gore, J. Katon, M.H. Norman, Vanilloid receptor ligands and their use in treatments, US 050176726-A1, 2005.
[68] C. Balan, N. Chen, E.M. Doherty, V.K. Gore, M.H. Norman, H.L. Wang, Vanilloid receptor ligands and their use in treatments, US 050182067-A1, 2005.
[69] http://clinicaltrials.gov/ct2/show/NCT00387140, accessed 17 May 2012.
[70] R. Bakthavatchalam, C.A. Blum, H.L. Brielmann, T.M. Caldwell, S. De Lombaert, Substituted Quinazolin-4-ylamine analogues, WO 03062209-A2, 2003.
[71] http://www.clinicaltrials.jp/user/showCteDetailE.jsp?japicId=JapicCTI-101177
[72] Y. Koga, S. Yata, T. Watanabe, T. Matsuo, T. Yamasaki, M. Sakata, W. Kondo, H. Ozeki, Y. Hori, Fused benzamide compound and vanilloid receptor 1 (VR1) activity inhibitor, WO 06006741-A1, 2006.
[73] S.M. Westaway, M. Thompson, H.K. Rami, G. Stemp, L.S. Trouw, D.J. Mitchell, J.T. Seal, S.J. Medhurst, S.C. Lappin, J. Biggs, J. Wright, S. Arpino, J.C. Jerman, J.E. Cryan, V. Holland, K.Y. Winborn, T. Coleman, A.J. Stevens, J.B. Davis, M.J. Gunthorpe, Design and synthesis of 6-phenylnicotinamide derivatives as antagonists of TRPV1, Bioorg. Med. Chem. Lett. 18 (2008) 5609–5613.
[74] G.J. Macdonald, D.J. Mitchell, H.K. Rami, L.S. Trouw, M. Thompson, S.M. Westaway, Carboxamide Derivatives, WO 04072069-A1, 2004.
[75] H. Uchida, N. Kosuga, T. Satoh, D. Hotta, T. Kamino, Y. Maeda, K. Amano, Y. Akada, Novel heterocyclidene acetamide derivative, WO 07010383-A1, 2007.
[76] H. Uchida, S. Ogawa, M. Makabe, Y. Maeda, Heterocyclidene-*N*-(aryl)acetamide derivative, WO 08091021-A1, 2008.
[77] L. Dubois, Y. Evanno, A. Malanda, *N*-(arylalkyl)-1*H*-pyrrolopyridine-2-carboxamide derivatives, preparation and therapeutic use thereof, WO 07010138-A2 and WO 07010138-A3, 2007.
[78] L. Horoszok, C. Leung, M. Tomaszewski, C. Walpole, New compounds I, WO 07091948-A2 and WO 07091948-A3, 2007.
[79] A. Gomtsyan, E.K. Bayburt, R.G. Schmidt, C.S. Surowy, P. Honore, K.C. Marsh, S.M. Hannick, H.A. McDonald, J.M. Wetter, J.P. Sullivan, M.F. Jarvis, C.R. Faltynek, C.H. Lee, Identification of (*R*)-1-(5-*tert*-Butyl-23-dihydro-1H-inden-1-yl)-3-(1H-indazol-4-yl)urea (ABT-102) as a potent TRPV1 antagonist for pain management, J. Med. Chem. 51 (2008) 392–395.
[80] A. Gomtsyan, E.K. Bayburt, J.R. Koenig, C.H. Lee, Fused compounds that inhibit vanilloid receptor subtype 1 (VR1) receptor, US 040254188-A1, 2004.
[81] C.S. Surowy, T.R. Neelands, B.R. Bianchi, S. McGaraughty, R. El Kouhen, P. Han, K.L. Chu, H.A. McDonald, M. Vos, W. Niforatos, E.K. Bayburt, A. Gomtsyan, C.H. Lee, P. Honore, J.P. Sullivan, M.F. Jarvis, C.R. Faltynek, (*R*)-(5-*tert*-butyl-23-dihydro-1H-inden-1-yl)-3-(1H-indazol-4-yl)-urea (ABT-102) blocks polymodal activation of transient receptor potential vanilloid 1 receptors in vitro and heat-evoked firing of spinal dorsal horn neurons in vivo, J. Pharmacol. Exp. Ther. 326 (2008) 879–888.
[82] ClinicalTrials.gov identifier NCT00854659, accessed 17 May 2012.
[83] L.A. Gharat, U.M. Joshi, N.K. Joshi, Substituted benzofused derivatives and their use as vanilloid receptor ligands, WO 07042906-A1, 2007.
[84] A. Charrua, C.D. Cruz, S. Narayanan, L. Gharat, S. Gullapalli, F. Cruz, A. Avelino, GRC-6211, a new oral specific TRPV1 antagonist, decreases bladder overactivity and noxious bladder input in cystitis animal models, J. Urol. 181 (2009) 379–386.
[85] A. Kahraman, R.J. Morris, R.A. Laskowski, J.M. Thornton, Shape variation in protein binding pockets and their ligands, J. Mol. Biol. 368 (2007) 283–301.
[86] LigPrep, version 2.5, 2011, Schrödinger LLC, New York, NY 10036-4041.
[87] Epik, version 2.2, 2011, Schrödinger LLC, New York, NY 10036-4041.
[88] J.C. Shelley, A. Cholleti, L.L. Frye, J.R. Greenwood, M.R. Timlin, M. Uchiyama, Epik: a software program for pKa prediction and protonation state generation for druglike molecules, J. Comput. Aided Mol. Des. 21 (2007) 681–691.
[89] J.R. Greenwood, D. Calkins, A.P. Sullivan, J.C. Shelley, Towards the comprehensive, rapid, and accurate prediction of the favorable tautomeric states of drug-like molecules in aqueous solution, J. Comput. Aided Mol. Des. 24 (2010) 591–604.
[90] W.L. Jorgensen, J. Tirado-Rives, The OPLS [optimized potentials for liquid simulations] potential functions for proteins, energy minimizations for crystals of cyclic peptides and crambin, J. Am. Chem. Soc. 110 (1988) 1657–1666.
[91] W.L. Jorgensen, D.S. Maxwell, J. Tirado-Rives, Development and testing of the OPLS all-atom force field on conformational energetics and properties of organic liquids, J. Am. Chem. Soc. 118 (1996) 11225–11235.
[92] G.A. Kaminski, R.A. Friesner, J. Tirado-Rives, W.L. Jorgensen, Evaluation and reparametrization of the OPLS-AA force field for proteins via comparison with accurate quantum chemical calculations on peptides, J. Phys. Chem. B 105 (2001) 6474–6487.
[93] MacroModel, version 9.9, 2011, Schrödinger LLC, New York, NY 10036-4041.
[94] W.C. Still, A. Tempczyk, R.C. Hawley, T. Hendrickson, Semianalytic treatment of solvation for molecular mechanics and dynamics, J. Am. Chem. Soc. 112 (1990) 6127–6129.
[95] G. Chang, W. Guida, W.C. Still, An internal coordinate Monte-Carlo method for searching conformational space, J. Am. Chem. Soc. 111 (1989) 4379–4386.
[96] M. Saunders, K.N. Houk, Y.D. Wu, W.C. Still, M. Lipton, G. Chang, W.C. Guida, Conformations of cycloheptadecane: a comparison of methods for conformational searching, J. Am. Chem. Soc. 112 (1990) 1419–1427.
[97] I. Kolossváry, W.C. Guida, Low Mode Search. An efficient automated computational method for conformational analysis: application to cyclic and acyclic alkanes and cyclic peptides, J. Am. Chem. Soc. 118 (1996) 5011–5019.
[98] I. Kolossváry, W.C. Guida, Low-mode conformational search elucidated. Application to C39H80 and flexible docking of 9-deazaguanine inhibitors to PNP, J. Comput. Chem. 20 (1999) 1671–1684.
[99] R.A. Jarvis, E.A. Patrick, Clustering using a similarity measure based on shared nearest neighbors, IEEE Trans. Comput. C-22 (1973) 1025–1034.
[100] A. Golbraikh, A. Tropsha, Predicitve QSAR modeling based on diversity sampling of experimental datasets for the test and training set selection, J. Comput. Aided Mol. Des. 160 (2002) 356–369.
[101] A.R. Leach, V.J. Gillet, An Introduction to Chemoinformatics, revised edition, Springer, Dordrecht, The Netherlands, 2007, pp. 121–123.
[102] Canvas, version 1.5, 2012, Schrödinger, LLC, New York, NY 10036-4041.
[103] V.N. Viswanadhan, H. Rajesh, V.N. Balaji, Atom type preferences, structural diversity, and property profiles of known drugs, leads, and nondrugs: a comparative assessment, ACS Comb. Sci. 13 (2011) 327–336.